Materials research at the Defence Metallurgical Research Laboratory

P. Rama Rao

Introduction

Defence Metallurgical Research Laboratory (DMRL), Hyderabad, is a major materials research establishment under the Defence Research and Development Organization. The genesis of the laboratory lies in the formation of the Technical Development Establishment (Metallurgical) at Ichapur near Calcutta four decades ago in 1950. DMRL, as it is known today, may be said to have come into being in 1963 (15 October 1963) as a result of the bifurcation that separated R&D from defence inspection in recognition of the need to set up a wholly dedicated research laboratory for materials development. The mandate of the laboratory consists of three aspects: (i) R&D for generation of new materials and technologies for defence hardware; (ii) R&D on futuristic materials, products and processes so as to provide the country with advanced technology options; (iii) metallurgical investigation coverage to the Services (Army, Navy and Air Force). This mandate, as well as the evolutionary aspect of the scientific elements of the materials discipline, underlies the ethos of DMRL R&D work, which may be described as *grafting new alloy technology on growing metal science.*

In regard to fulfilling the mandate in specific terms, DMRL's accomplishments have included critical product supply (e.g. tungsten carbide ammunition components, light alloy castings for aerospace agencies, magnets for rocket launchers, oxygen-free high-conductivity copper for pressue gauges, to name a few); technology transfer (such as for the manufacture of aircraft brake pads, clutch discs for heavy military vehicles, tungsten alloy-based antitank ammunition, steel core antitank ammunition, steel and composite armours, to name the major ones), and a large number of metallurgical investigations of various types for selective indigenization of defence hardware (e.g. torpedo suspension bands, transmission shaft for the armoured personnel carrier, brazed heat sinks for mounting electronic componets) as well as for the understanding and prevention of the failure of components (e.g. MIG 23 aeroengine blade failure, rocket motor casing failure).

Reactive metal extraction represents a gap area in the indigenous metallurgical R&D scenario. DMRL has focused upon this field and has set up demonstration plants for extraction of titanium and magnesium. Based on this work the Government of India has in principle taken a decision to set up a 1000 ton titanium sponge processing plant in India. Extraction facilities for making neodymium and lithium are also in an advanced stage of being established.

Recognizing the importance of materials processing for component development, DMRL has set up a range of facilities which are complementary to those existing elsewhere within the country. Facilities for isothermal forging, superplastic forming, electroslag casting, inert gas atomization, cold and hot isostatic pressing, laser processing, light alloy castings, directional solidification and single-crystal component castings may be cited in this context. Thus, development of the complex technologies for special product processing (like the directionally solidified and single-crystal aeroengine turbine blades, powder processed integral blade-disc missile component and the titanium alloy air bottles) has been a thrust area in DMRL. Emphasis currently is laid on analysis of the scientific issues underlying these processes for optimizing process controls and achieving higher quality products. Computer simulation and modelling is a part of the new approach employed to optimize process and component manufacture.

It is noteworthy that DMRL has over the years successfully contributed to the creation of new institutions to serve specific areas of high technology for defence as well as civilian applications. Four such major institutions have come into existence through the initiative of DMRL during the last 15 years. These are (i) the Mishra Dhatu Nigam Limited, Hyderabad, for manufacture of special steels, superalloys, titanium alloys and refractory metals meeting stringent quality specifications; (ii) the Heavy Alloy Penetrator Project located at Tiruchirapalli for manufacture of tungsten alloy-based antitank ammunition—the first Ordnance Factory to come up on the basis of indigenous design and technology; (iii) Non-Ferrous Materials Technology Development Centre (NFTDC) which is an unique venture supported by four public sector undertakings, namely Hindustan Copper Limited, Hindustan Zinc Limited, National Aluminium Company Limited and Bharat Aluminium Company Limited with DMRL acting as the nodal agency. The primary objective of the Centre, which has brought about cooperative R&D between the industry and a defence laboratory, is to promote speciality nonferrous materials development for industrial and commercial exploitation, (iv) Indo-Soviet Advanced Research Centre for Powder Metallurgy for which sanction has just been accorded by the Government. This will be located at Hyderabad and devoted to promote product development based on powder processing in collaboration with the Soviet Union under the umbrella of the Integrated Long-Term Programme of Cooperation in Science and Technology between India and USSR. DMRL and Byelorussian Powder Metallurgy Association will act as the nodal implementing institutions. The Department of Science and Technology, Government of India, will be the supporting nodal Government Department.

DMRL's research programmes are aimed at gaining a scientific understand-

P. Rama Rao is Director, Defence Metallurgical Research Laboratory, Hyderabad 500 258.

ing of the materials development from the stage of selecting their chemical composition, their processing, characterization and conversion to components. Some recent results which are an outcome of the on-going projects are presented in the following sections

Current research activities in advanced materials

Intermetallics

Titanium aluminides. The intermetallic Ti_3Al possesses high-temperature properties substantially superior to those of the conventional titanium alloys but is extremely brittle. The last decade has seen the development of Ti_3Al-based alloys with acceptable room temperature plasticity and these alloys are now on the threshold of commercial exploitation by the aerospace industry. The design of such alloys is essentially based on the principle of stabilizing the high-temperature ductile bcc phase of titanium (β) through alloying. Niobium has found favour as the preferred β stabilizer since it also results in beneficial changes in the nature of slip.

At DMRL, the critical issue of room temperature plasticity in Ti_3Al–Nb alloys has been investigated through a series of experiments designed to understand the role of microstructure (the shape, size, distribution and volume fraction of the constituent phases of these alloys) and the intrinsic effect of Nb in solid solution. The analyses include the characterization of the failure initiation and propagation mechanisms as influenced by the effect of structure on the micromechanisms of plastic flow. Such an analysis reveals[1-3] that ductility is achieved primarily by delaying the onset of cleavage crack nucleation in Ti_3Al by relaxation of the stress concentration at Ti_3Al grain boundaries by the ductile β phase (Figure 1). At volume fractions above 20% the β-phase will retard crack extension as well.

Work at DMRL has also explored the effect of Nb on phase equilibria and transformations along the $(Ti_xNb_{1-x})_3Al$ section of the ternary system Advanced techniques of analytical electron microscopy, such as convergent-beam electron diffraction and channelling-enhanced microanalysis have been utilized to show that Ti_3Al enriched with Nb possesses an orthorhombic rather than the hexagonal symmetry[4] and that the β-phase orders to a B2 structure (Figure 2). The site occupation of various atomic species in these ordered structures has also been determined[5,6]. The phase spaces which arise as a consequence have been identified[7] and an exploration of the thermodynamic factors which underlie these phase equilibria is in progress[8].

Mechanisms of creep in two phase Ti_3Al–Nb alloys in the temperature regime of interest have been determined[9]. Figure 3 shows the transition from diffusional creep to dislocation creep with increasing stress at 650 C and also indicates the strong effect of the morphology of the Ti_3Al shape on creep resistance The improved creep strength of these multicomponent intermetallic alloys compared to disordered hcp titanium is primarily due to a reduction, by about two orders of magnitude, of the frequency factor in both lattice and grain boundary diffusion as a result of ordering.

Figure 4 illustrates the specific strength as a function of temperature of a typical Ti_3Al base composition developed at DMRL[10] in comparison with a nickel-base superalloy INCO 718 and a modern commerical high-temperature titanium alloy, IMI 834 The retention of strength in the Ti_3Al alloy to a temperature as high as 700 C is noteworthy

Nickel aluminides. It is well established that the flow stress of ordered nickel aluminide and its alloys exhibits an

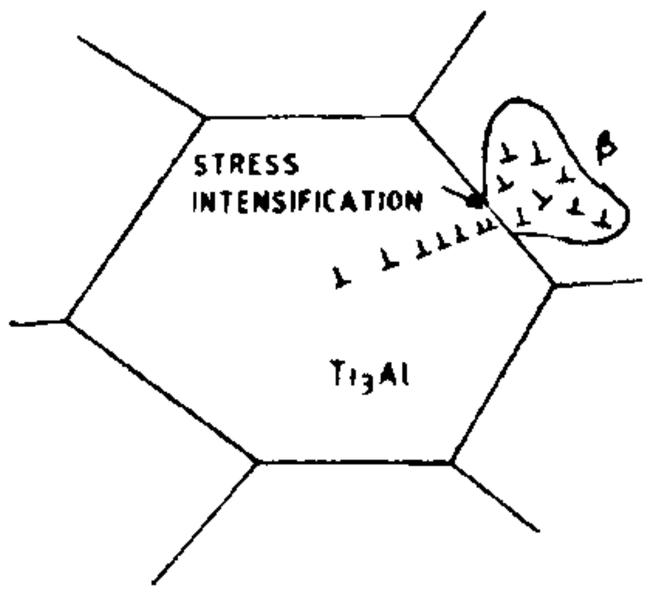

Figure 1. A schematic description of stress intensification at Ti_3Al grain boundaries due to anisotropy and inhomogeneity of slip in this phase The stress concentration can be relieved by a second phase which deforms in a more isotropic manner.

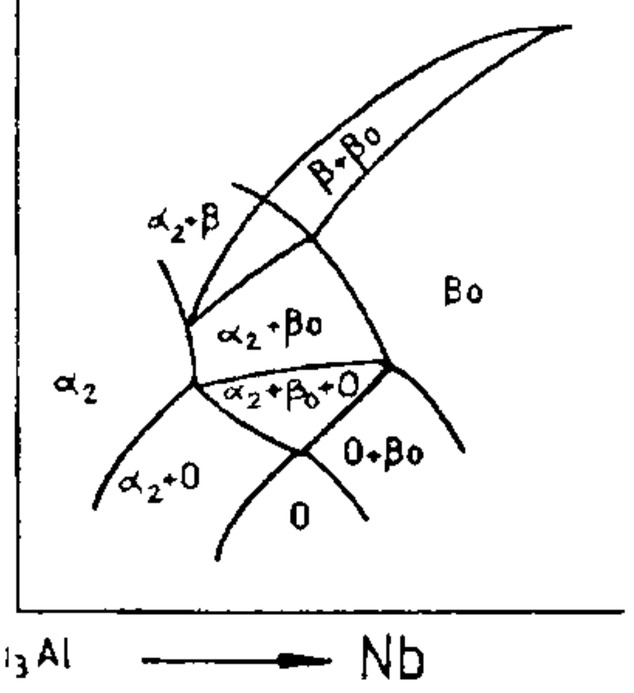

Figure 2. Phase spaces in the $(Ti_xNb_{1-x})_3Al$ section

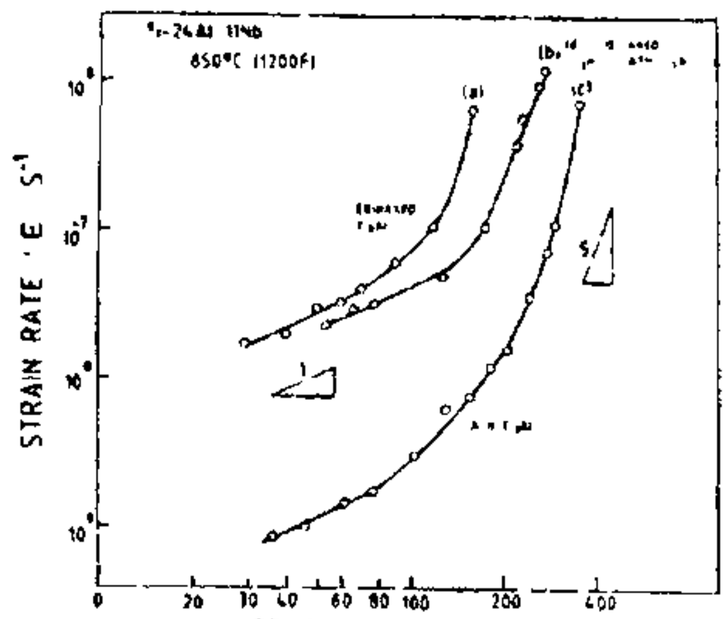

Figure 3. Stress-strain rate plot of a Ti_3Al base alloy as a function of microstructure. A transition from diffusional creep (stress exponent or slope equal to 1) to dislocation creep (stress exponent or slope equal to 5) is observed The aspect ratio of the Ti_3Al grains strongly influences creep strength

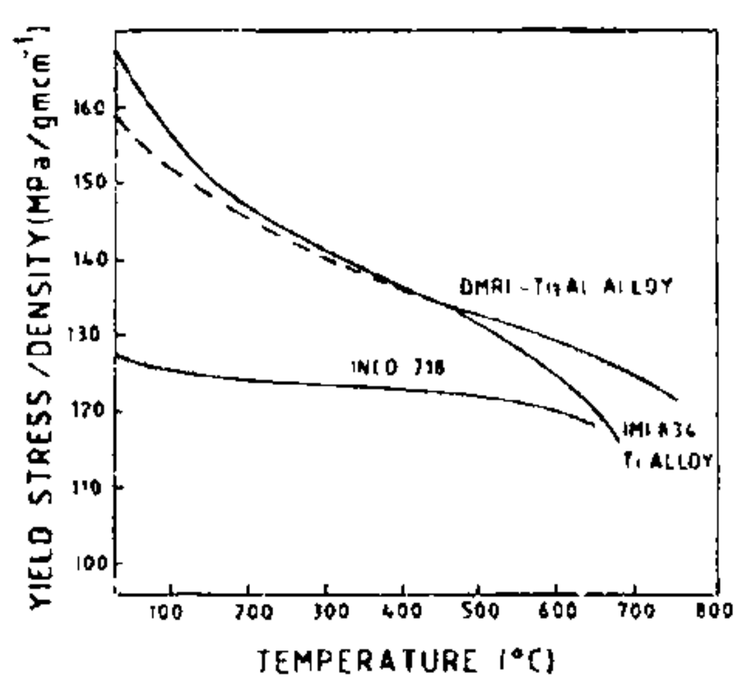

Figure 4. The specific yield stress of a DMRL-Ti_3Al base alloy compared with a Ni base superalloy (INCO 718) and the most advanced high-temperature titanium alloy (IMI 834) currently available commercially

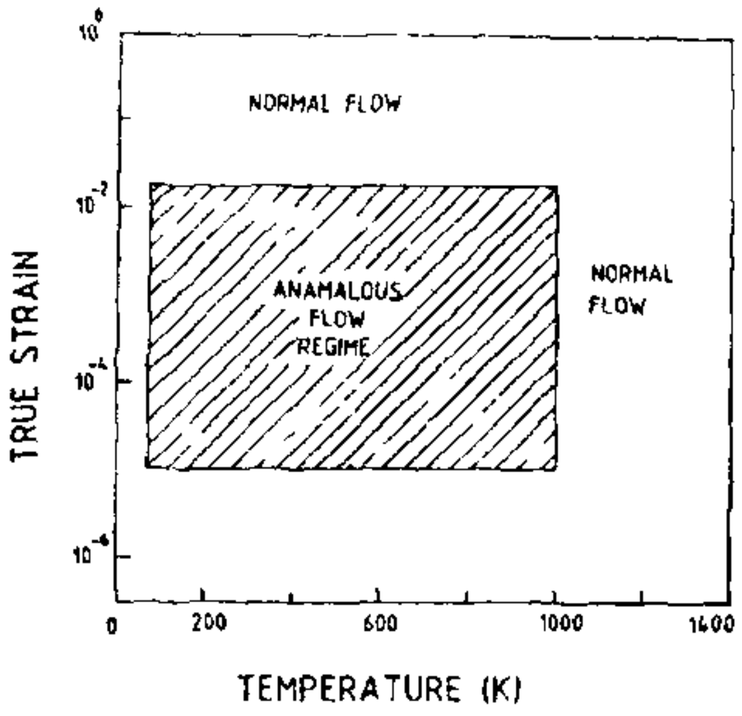

Figure 5. The true strain–temperature plot for Ni_3Al indicating the bounded region (shaded) exhibiting anomalous flow behaviour.

anomalous increase with increasing temperature[11]. Recent work at DMRL has shown that the anomaly in the flow stress-temperature behaviour disappears beyond about 2% strain in the case of directionally solidified nickel aluminides[12]. This result, in conjunction with the literature data, indicates a closed region in the temperature–true strain space, as illustrated in Figure 5, only within which the yield and flow behaviour of Ni_3Al is anomalous.

Nickel alloys

Nickel-base superalloys are extensively used as a structural material in aircraft gas turbine engines because of their exceptional creep resistance at elevated temperatures. Some of the most critical components like the gas turbine blades and discs are currently made from advanced nickel-base superalloys. If we consider the blade profile, it is seen that these superalloys have to be shaped to complex forms and with different section sizes. DMRL is engaged in research concerned with the problem of creep embrittlement that nickel-base superalloys suffer in oxygen (air) environment, if the oxide scale is either absent or does not form with sufficient rapidity[13–15]. Under such conditions, the creep embrittlement becomes particularly important in investment cast components having thin section size. To study this effect, creep tests were conducted on an Inconel X-750 nickel-base alloy using three different geometries –solid, flat and tubular. It was observed that time-to-fracture was progressively shortened as the specimen thickness was reduced[16] (Figure 6,*a*). The creep behaviour exhibited by the alloy in the three specimen geometries was compared on the basis of similar section size. It emerged that the times-to-rupture of tubular specimens were considerably longer than those of the flat and the solid specimens (Figure 6,*a*) while the minimum creep rate at all the applied stresses was found to be nearly unaffected by the specimen geometry. It was further noted that the equivalence of creep life data with different geometries can be obtained if the comparision is made at a constant value of the ratio of the cross-sectional area to the perimeter (Figure 6,*b*).

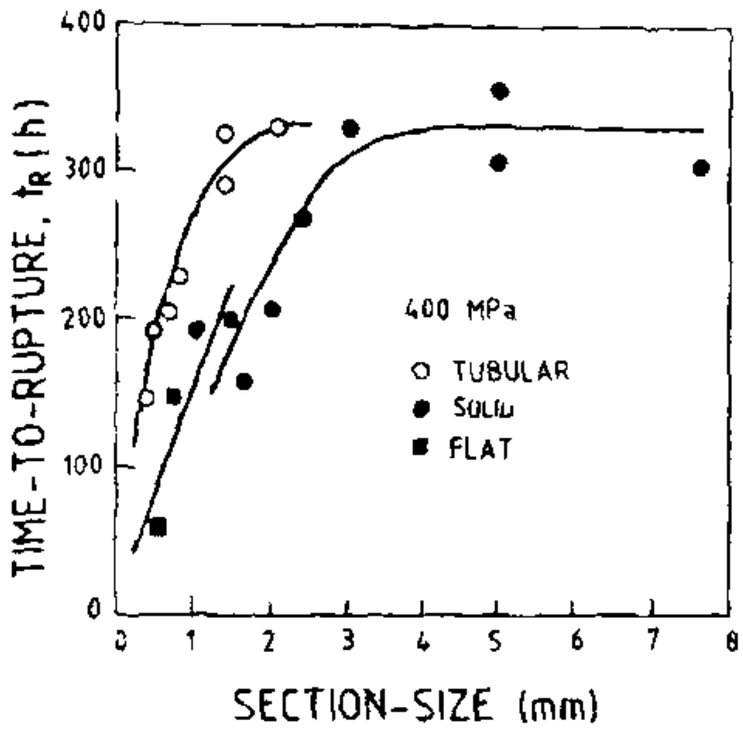

Figure 6, *a*. Time-to-rupture as a function of section size for nickel base superalloy specimens of different geometries.

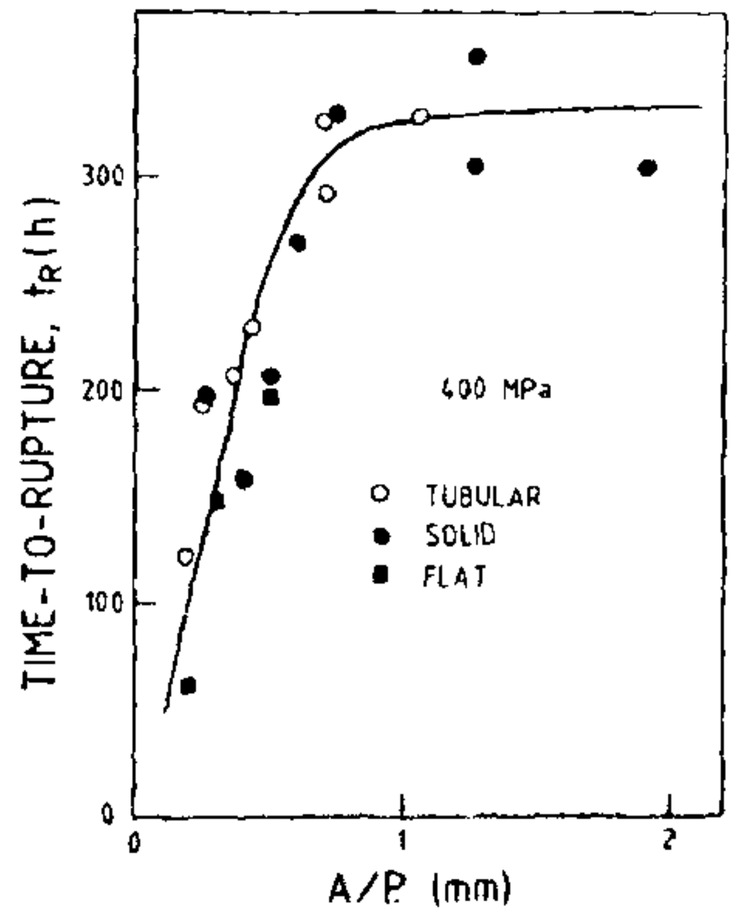

Figure 6, *b*. Time-to-rupture as a function of ratio of cross-sectional area to the perimeter for nickel-base superalloy specimens of different geometries.

Ultra-light alloys

Magnesium–lithium alloys which have a very low density ($\sim 1.36\ g\ cm^{-3}$) are now finding increasing usage in the aerospace industry since they offer up to 25% weight savings over the conventional magnesium alloys. Melting and casting procedure for the highly reactive Mg–Li alloy has been optimized at DMRL[17]. These alloys are being currently used mainly for non-structural applications, since their full-scale commercial development has been impeded by their poor creep resistance. Recent work at DMRL[18] has shown that the creep resistance of a Mg–Li–Al alloy can be substantially improved by minor additions of zirconium (Figure 7).

Aluminium–lithium alloys

High specific stiffness and strength compared to the conventional aluminium alloys has spurred the development of Al–Li alloys worldwide for aerospace applications. DMRL, in line with the above trend, has taken on a major programme for the development of Al–Li alloys. Substantial work has been carried out to optimize the microstructure through appropriate choice of melting, casting, processing and heat treatment schedules[19,20].

Al–Li alloys exhibit considerable degree of anisotropy in mechanical properties due to a strong texture and an aligned grain structure. A recent study

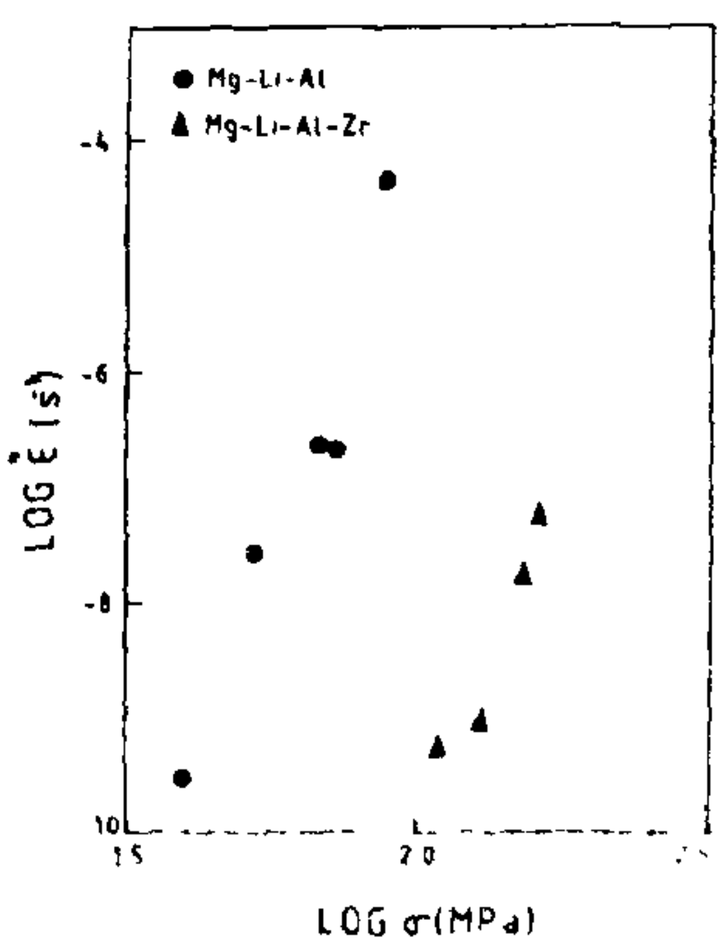

Figure 7. The effect of zirconium addition on the room temperature creep behaviour of Mg–Li alloys

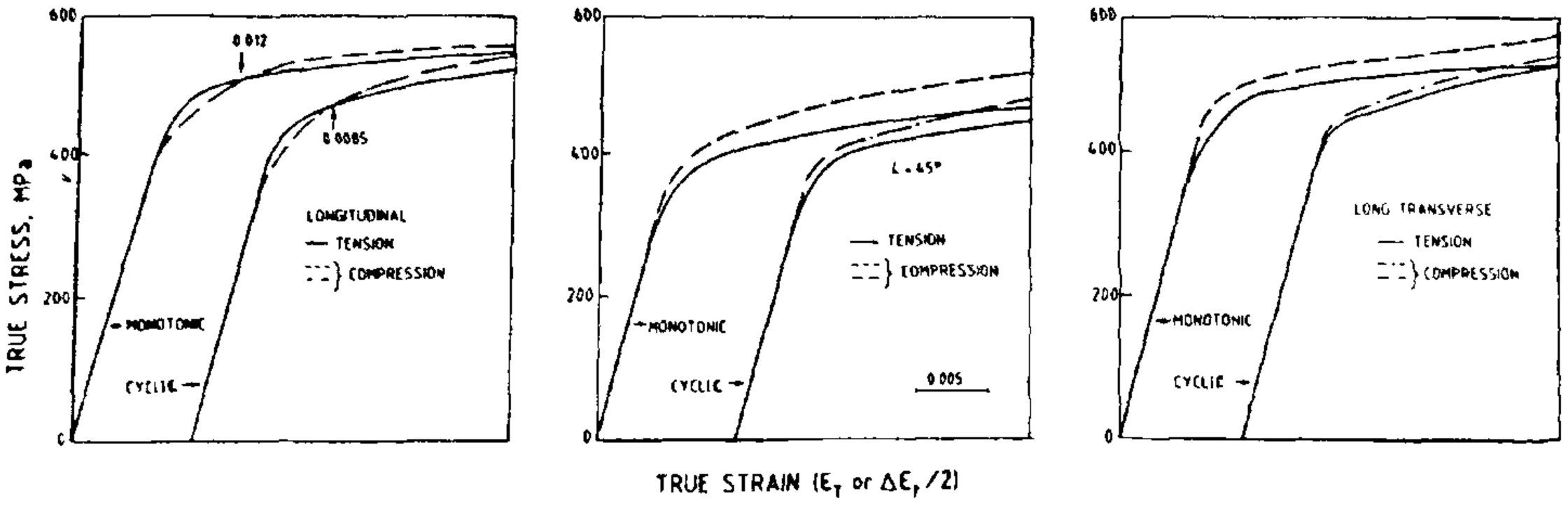

Figure 8. The strength differential effect in Al–Li alloys under monotonic and cyclic loading conditions.

conducted at DMRL on a quaternary Al–Li alloy Alcan 8090 in T8E51 condition to determine the anisotropy in mechanical properties has revealed the existence of a 'strength differential (SD)', which is seen to be directional[21]. The results from low cycle fatigue and tensile tests are presented in Figure 8. The Al–Li alloy in the longitudinal direction exhibits a lower compressive flow stress compared to the tensile flow stress (Bauschinger effect) at low strains. The stretch given to Al–Li alloys during processing to enhance the precipitation of S phase is responsible for this behaviour. However, the SD effect, characterized by a compressive flow stress higher than the tensile flow stress, prevails at all strain levels in the L+45° and LT (L+90°) directions (see Figure 8) and at higher strains in the L orientation.

Metal matrix composites

As a part of the detailed research programme at DMRL to evaluate the influence of materials as well as process-related variables on the mechanical behaviour of aluminium matrix composites, the specific influence of the type of reinforcement on the mechanical behaviour of both aluminium and 2124 alloy matrix has been investigated. Four different reinforcements (20% volume fraction), namely TiC, B_4C and TiB_2, were added, to the aluminium or 2124 alloy matrix. It is clear from Figure 9 that TiC is the most effective among the four reinforcements in both aluminium and Al 2124 alloy matrix. Continuing work at DMRL[22] on Al–TiC composite has resulted in the finding that a substantial improvement in strength levels (up to 67% increase in UTS) and hardness (up to 80%) can be achieved by subjecting this composite to a special thermal treatment. The increase in strength is mainly due to the significant refinement of the microstructure as illustrated in Figure 10.

Al–SiC composites show dissimilar creep behaviour when tested in tension and compression[23] (Figure 11). In tension, because of the early onset of the tertiary stage, the minimum creep rate does not correspond to the true steady-state creep rate above a transition stress. From the measurement of change in density per unit strain to fracture, it appears that such a transition is associated with the relative contribution of cavitation and necking to the fracture process; below the transition stress, cavitation seems to be dominant whereas necking is observed above the transition stress[23].

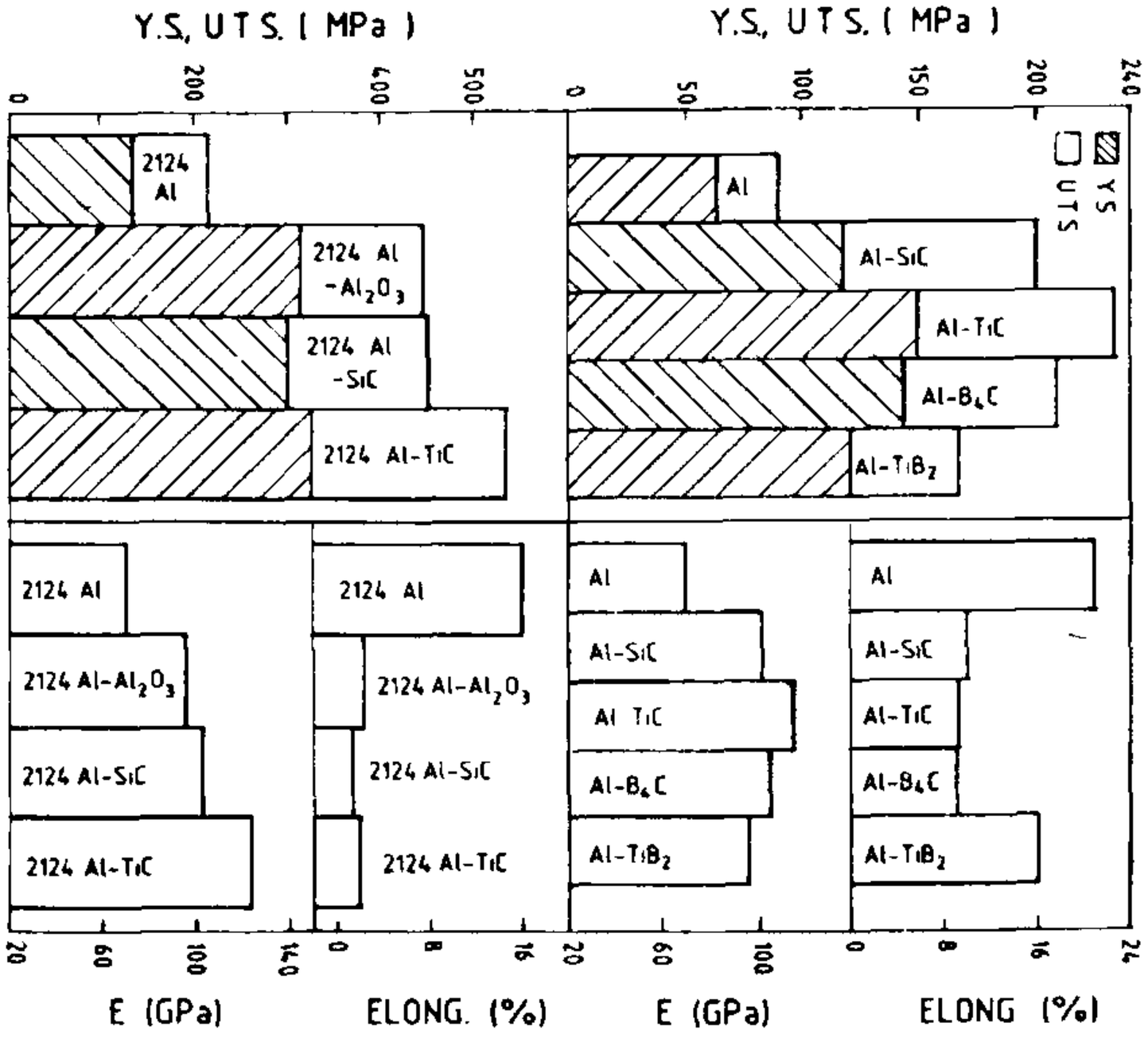

Figure 9. The effect of particulate reinforcement on the mechanical behaviour of aluminium composites.

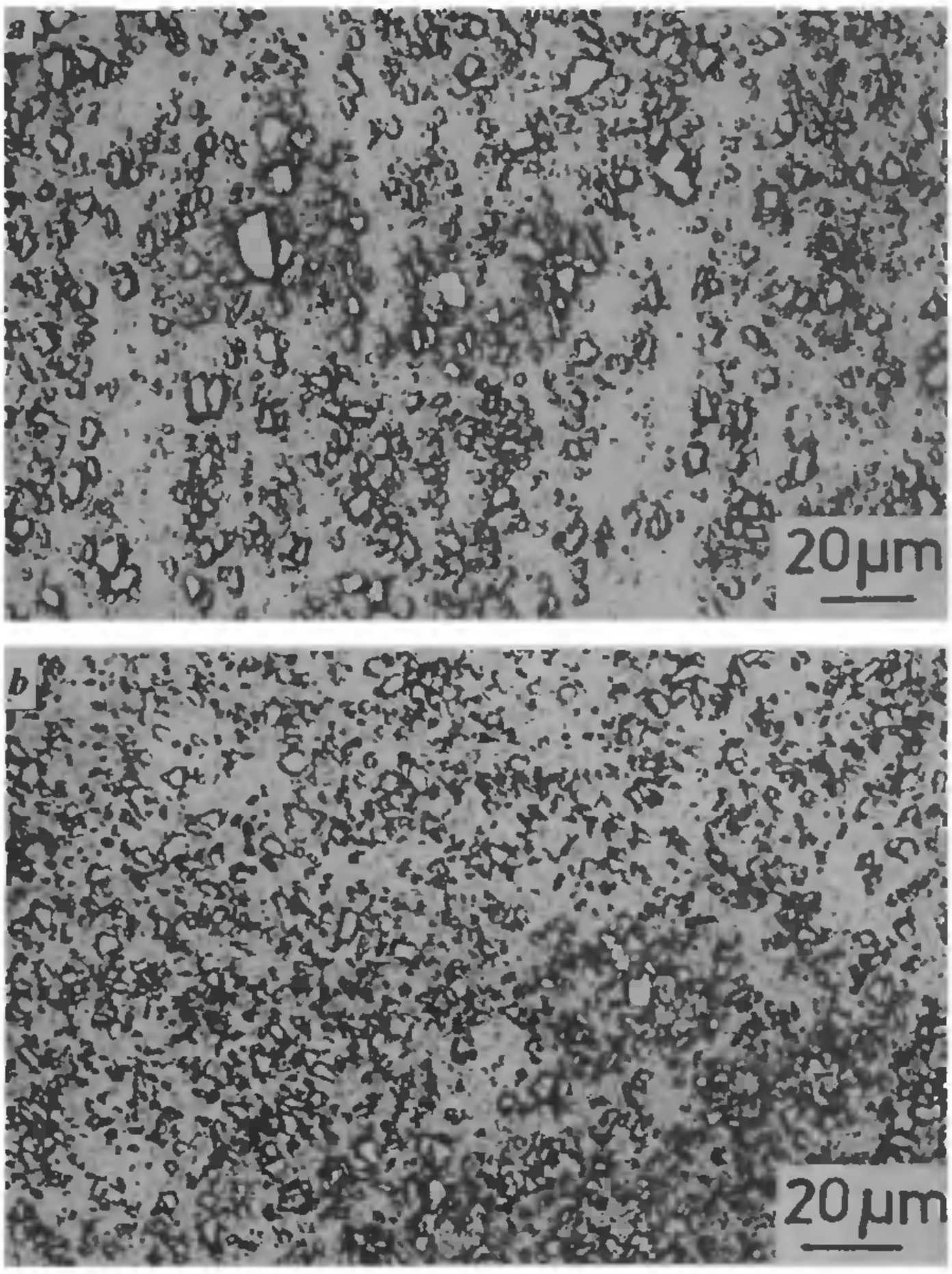

Figure 10. Optical micrographs of Al–20 vol.% TiC composite. (*a*), as hot-rolled (*b*), subjected to special thermal treatment.

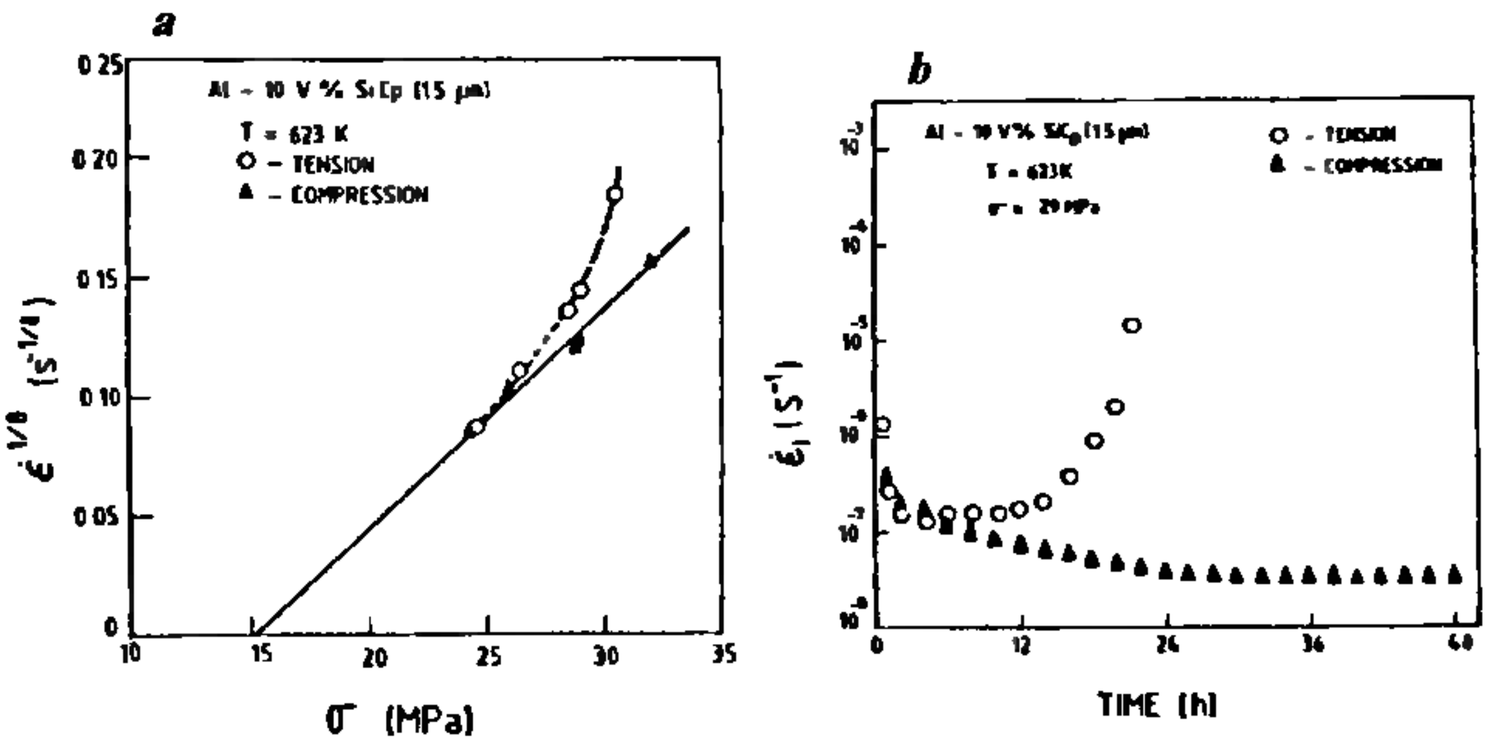

Figure 11. Creep behaviour of Al–SiC composite under tension and compression. (*a*), $\dot{\varepsilon}^{1/8}$ against applied stress, (*b*), variation of instantaneous strain rate with time showing that the minimum creep rate in tension does not correspond with steady-state creep rate in compression.

High energy magnets

A major research programme to develop Nd–Fe–B magnetic materials has been launched at DMRL in view of the fact that India has large resources of rare earths. A primary requirement for obtaining high coercivity in Nd–Fe–B alloys is a fine grain structure of the ferromagnetic phase surrounded by a non-magnetic Nd-rich phase at grain boundaries. Such a 'composite' structure prevents domain wall displacement and rotation and postpones nucleation of reverse domains leading to high coercivity. Figure 12 illustrates the typical microstructure of the Nd–Fe–B alloy developed at DMRL. It shows grains of ferromagnetic $Nd_2Fe_{14}B$ phase (dark regions) almost insulated from each other by Nd-rich bright areas as required for high coercivity. Values for the energy product in excess of 30 MgOe have been consistently achieved.

Machinable glass-ceramics

In a mica-based glass-ceramic, machinability with conventional metal working tools is achieved when flourmica is the crystalline phase. Micas are sheet-structured silicates that are strong and cleavable. Interlocking microstructure of randomly oriented fine-sized crystallites confer machinability as these crystals deviate a crack and arrest microscopic fractures. A glass ceramic of K_2O–SiO_2–MgO–Al_2O_3–F composition was processed at DMRL through melt as well as gelation route. A hot-pressed gel powder was found comparable to commercial macor.

The advantages of gelation route rest in (i) high homogeneity, (ii) fine particle size, and the glass phase at temperatures lower compared to the melting point of oxides (1450°C).

In calcia–yttria–alumina–silica system a glassy silicate is obtained at 250°C. On further heat treatment, $Ca_4Y_6(SiO_4)_6$ crystals form above 900°C. These needle-shaped crystallites interlock (Figure 13) and give rise to good machinability in the glass-ceramic.

Plasma spray coatings

The major activity in plasma-sprayed coatings at DMRL is the development of thermal barrier coatings (TBC) on Ni-base superalloys for their use in aviation gas turbine engine parts, such as the

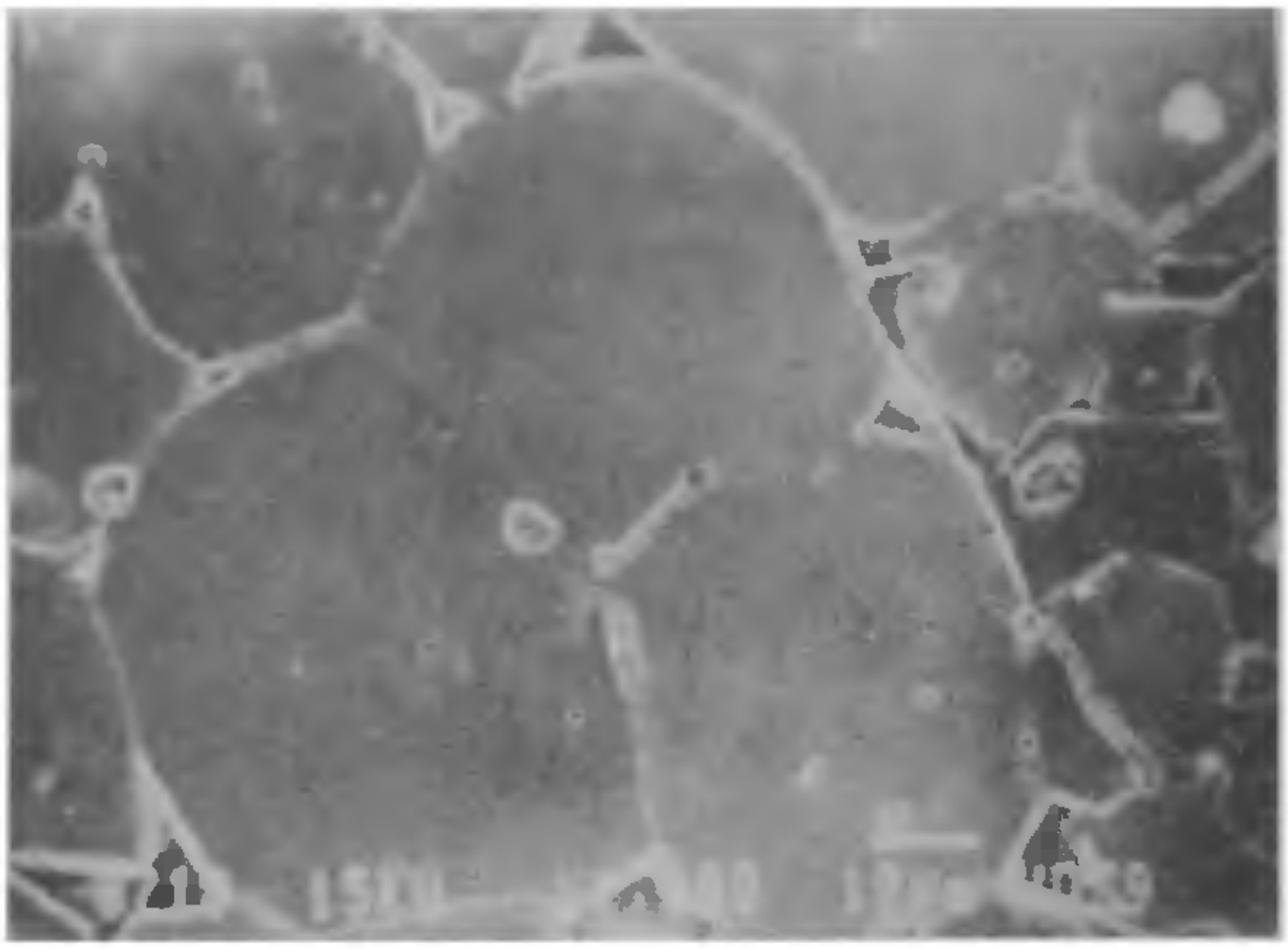

Figure 12. Microstructure of Nd–Fe–B magnetic alloy.

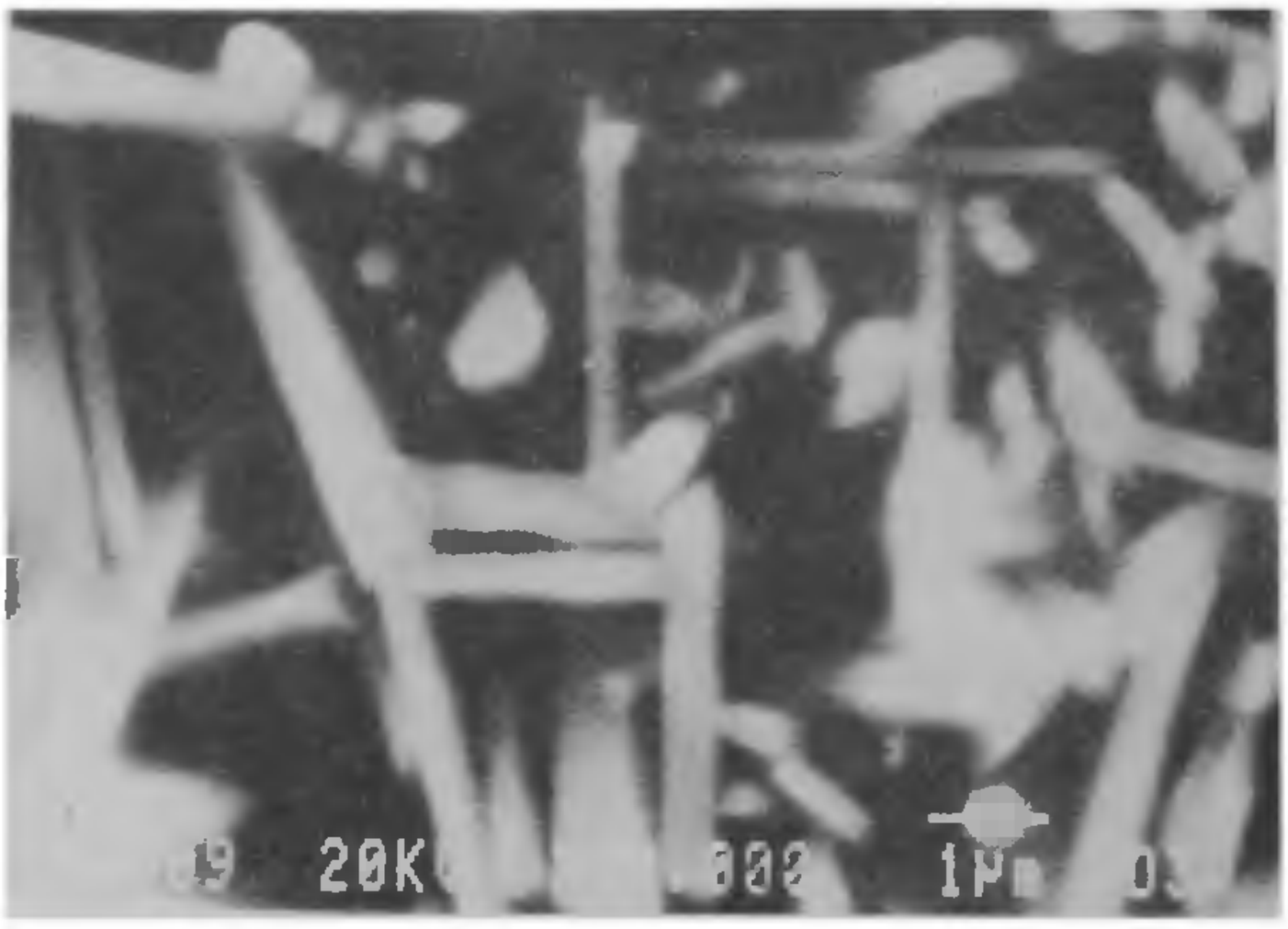

Figure 13. Interlocked crystallites of $Ca_4Y_6(SiO_4)_6(OH)_2$ in sintered glass ceramic.

combustion chamber and the after-burner. Efforts are also underway to develop insulative ceramic coatings to protect the turbine components, such as blades and vanes, at high temperatures.

As an integral part of the above programme and to evaluate the importance of the vaporization of the particle and the resultant particle size reduction during the plasma spraying process, modelling of the plasma–particle interaction has been carried out[24,25].

The reduction in the size of the particle due to vaporization, as predicted by the model, has been verified experimentally. This was done by plasma spraying the particles of a narrow size range in water and measuring the reduction in the average size of these sprayed particles. The experimental results corroborate the predictions of the model, as shown in Figure 14,*b*.

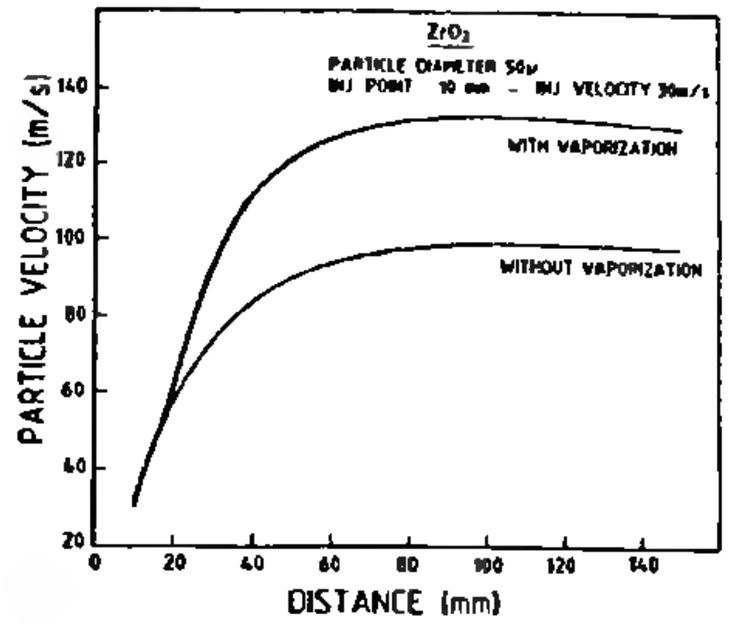

Figure 14, *a*. Variation of the velocity of a ZrO_2 particle of 50 μm diameter moving along the axis of an Ar/H_2 plasma flame

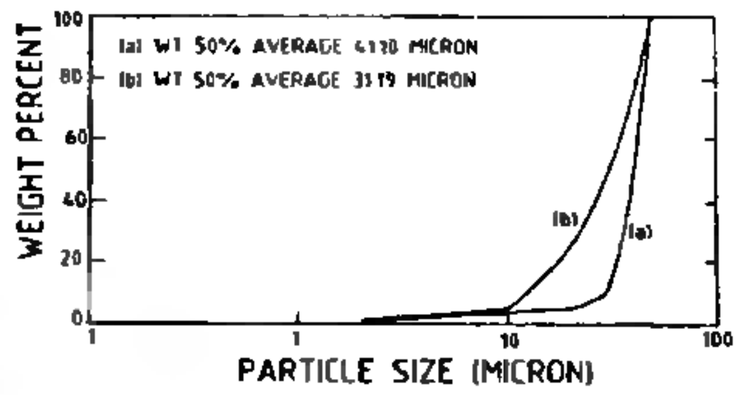

Figure 14, *b*. Particle size distribution of yttria stabilized zirconia powder (a) before, (b) after it was plasma sprayed in water.

Current research activities in advanced processing technologies

Metal-mould reactions in titanium castings

Casting technology is expected to provide a viable and economical route for producing near-net-shaped titanium components. However, special and expensive mould materials are required to alleviate/minimize the reactivity of titanium. In this regard a detailed study was recently attempted at DMRL to evolve a methodology for qualitative and quantitative evaluation of interfacial reactivity of titanium with mould materials during casting. Microhardness profiles and analysis of oxygen contamination provided an index for evaluation of the reactivity of titanium[26–28]. Microhardness profiles (Figure 15) delineated two distinct regions, one of which is characterized by a low value of hardness which is invariant with distance. The reaction products are uniformly distributed in this region. The second region is characterized by a sharp decrease in microhardness with distance from the metal-mould interface. This region represents a diffusion zone for solutes that dissolve into titanium from the mould. The composition-depth profiles (Figure 16) determined by scanning electron probe microanalyser in the as-cast titanium were found to be similar to those of the microhardness profiles (Figure 15), implying that microhard-

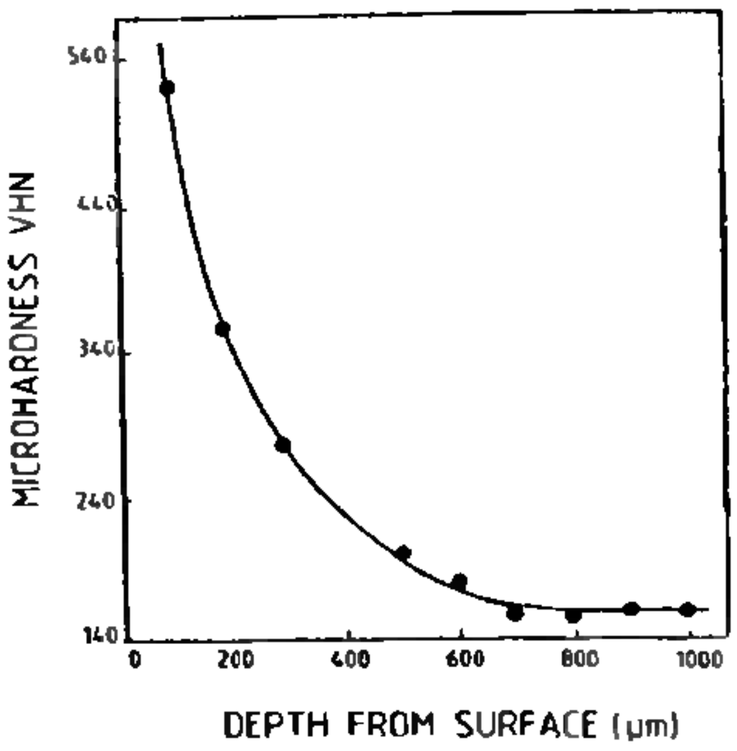

Figure 15. Microhardness as a function of distance from surface for titanium cast in sodium silicate-bonded zircon mould containing 7.5% ZrO_2 and fired at 1473 K.

ness can be considered as an index of the contamination resulting from the metal-mould reaction. This approach of evaluating reactivity was extended to determine the thermal stability of oxide face coats[29] against liquid titanium for the investment casting process. The relative stability of evaluated oxides, in the order of increasing stability, followed the sequence: CeO_2, ZrO_2, Gd_2O_3, didymium oxide, Sm_2O_3, Nd_2O_3 and Y_2O_3. The grading did not follow the free energy data of the formation of these oxides. A better correlation with experimental observations was obtained when the solubility of the metallic species in titanium was also taken into consideration[27].

Undercooled structures by rapid pressurization

In the rapid cooling techniques the melt is made to cool so rapidly that nucleation does not occur until the melt attains a high degree of undercooling. It was postulated that undercooling could result by rapidly shifting the equilibrium melting point to higher temperatures. According to Clausius–Clapeyron equation, equilibrium transformation temperature of any exothermic reaction increases with pressure if it is accompained by volume reduction. Solidification of majority of metals is one such example. In such materials rapid pressurization should produce significant undercooling.

This novel idea of rapid pressurization has been demonstrated on the Pb–Sn system[30]. Sn-30 wt% Pb alloy discs were initially pressurized to 0.5–1.0 GPa in an opposed anvil device with tungsten carbide anvils and heated to 10–20°C above the estimated melting point. Then the specimen was step loaded to the final pressure. The samples were then cooled before relaxing the pressure. Undercooling of the order of 0.1 T_m, where T_m is the liquidus temperature, were obtained and resulted in microstructures comparable to splat cooled samples, as illustrated in Figure 17. A merit of this technique is that it makes bulk undercooling possible.

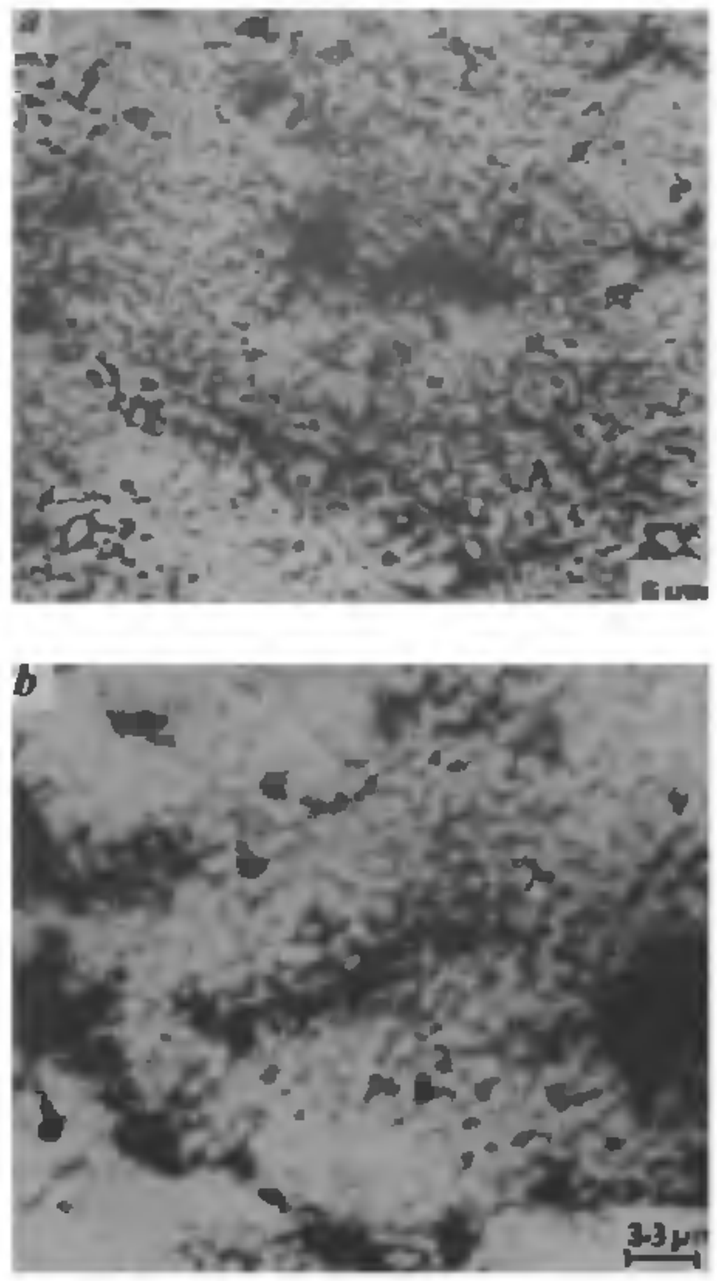

Figure 17. The similarity of the surface microstructures of the tin–lead alloys obtained using the conventional splat cooling (*a*), and rapid pressurization (*b*) techniques.

Processing of high T_c superconductors

The full potential of high-temperature superconductors like $YBa_2Cu_3O_7$ can be realized only if the problems related to their fabricability leading to low-current densities can be solved. The low current density is mainly due to the lack of an aligned microstructure and the presence of non-superconducting phases at grain boundaries or microcracks. Recent published work suggests that the above problems can be overcome in the case of the $YBa_2Cu_3O_7$ superconductor ($T_c = 92$ K) by the use of the 'melt growth process'. This process leads to an oriented microstructure and also eliminates the occurrence of non-superconducting phases at the grain boundaries. DMRL has adopted the melt growth process to the fabrication of $YBa_2Cu_3O_7$ material. Figure 18,*a* shows the aligned microstructure of $YBa_2Cu_3O_7$ obtained by the melt growth process while Figure 18,*b*, a micrograph obtained using polarized light, reveals the existence of parallel twin boundaries cutting across several grains.

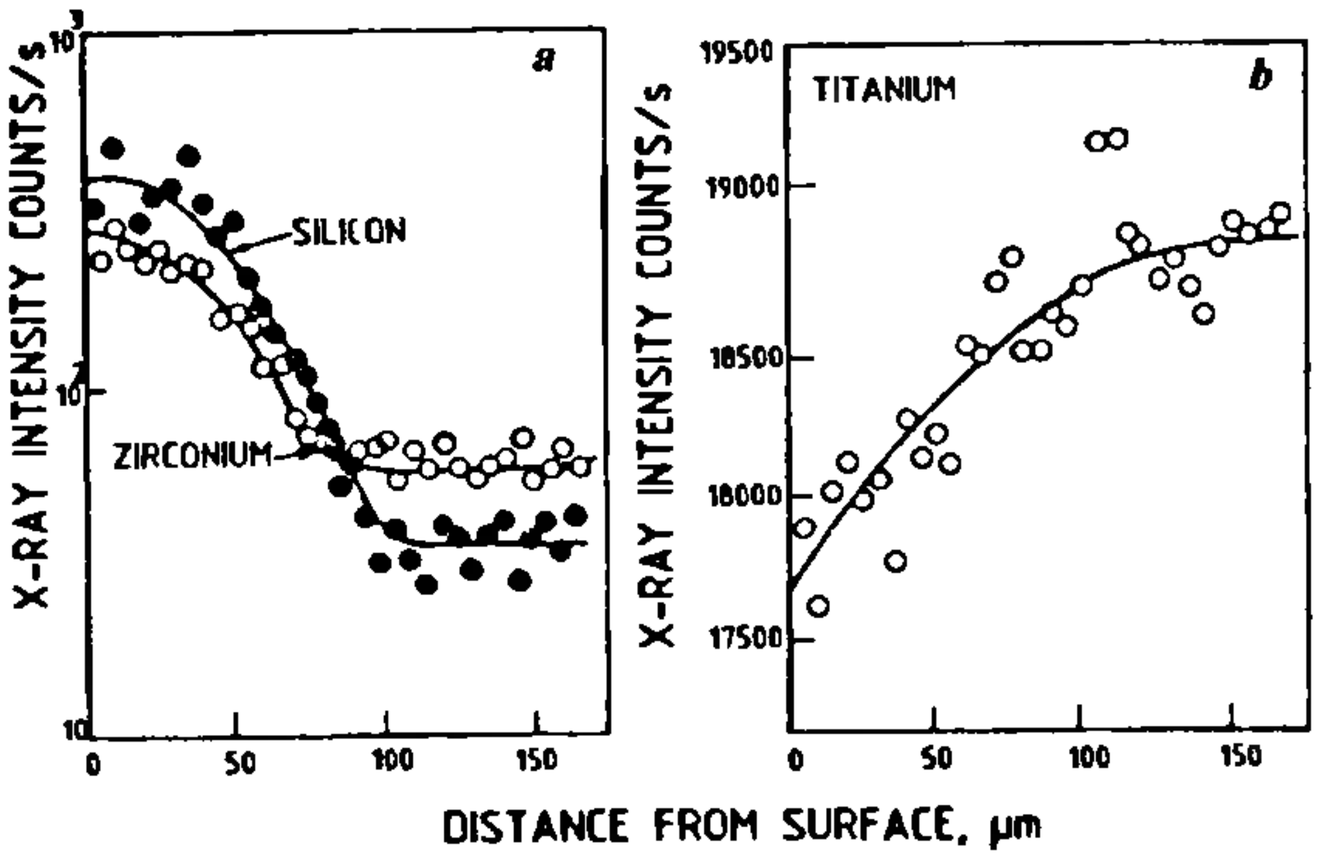

Figure 16. *a*, Composition depth profile showing diffusion of Zr and Si in the as-cast titanium at the metal (titanium) mould (ZrO_2) interface. *b*, Corresponding variation in titanium concentration.

Processing of nickel-base superalloys

The nickel-base superalloys are prone to segregation resulting in inhomogeneous

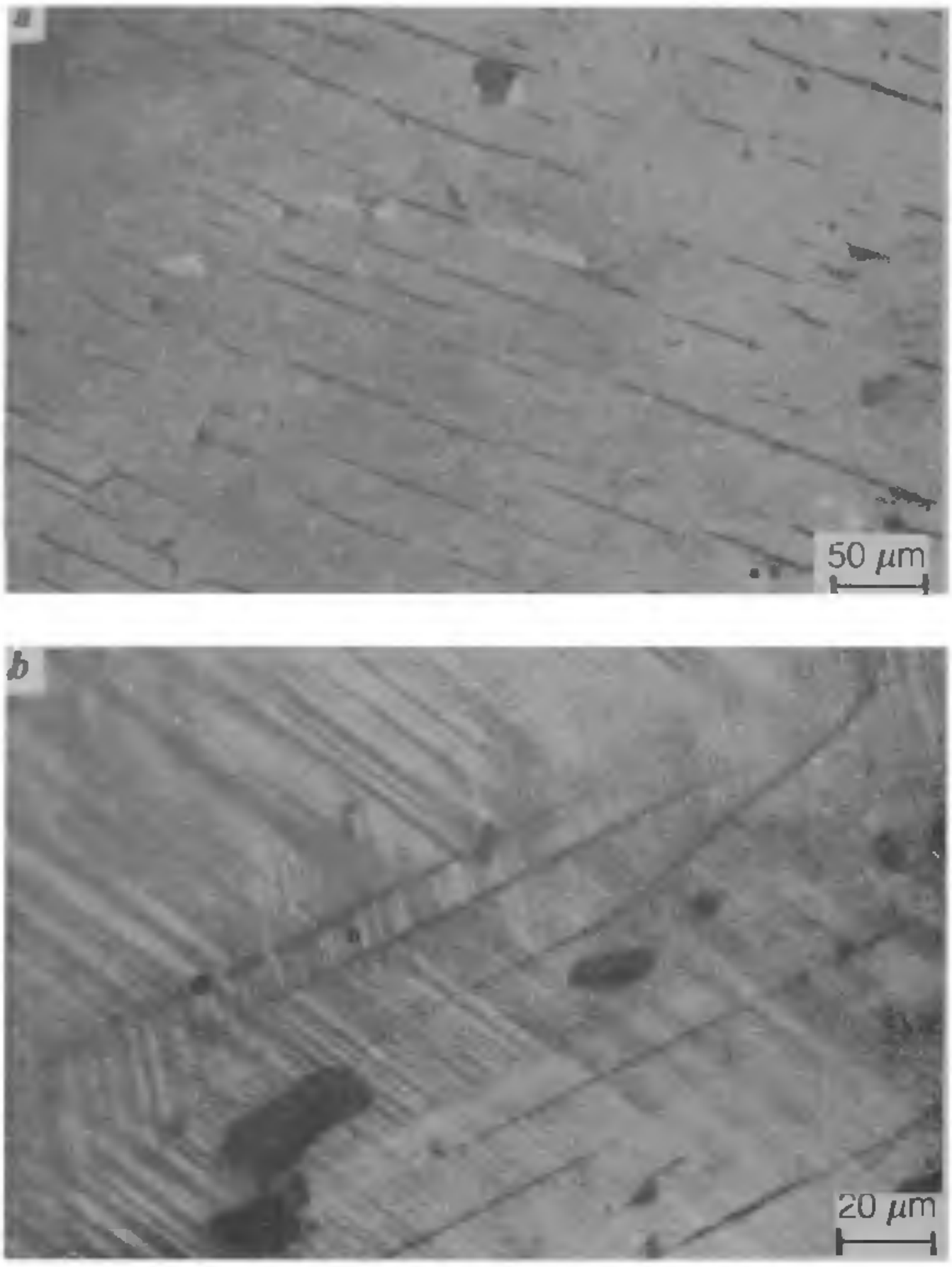

Figure 18. Alligned microstructure of $YBa_2Cu_3O_7$ superconductor using the melt growth process.

precipitation of carbides, if they are made by the conventional casting route. Consequently much effort has gone into processing these alloys through the powder route Prealloyed powders are usually sintered at high pressures and elevated temperatures in a hot isostatic press (HIP) and then subsequently forged. All aspects of the processing of nickel-base superalloys by the powder route have been reviewed recently[31].

At DMRL, the influence of HIP parameters on the microstructure and mechanical properties of a nickel-base superalloy (APK1) has been characterized[32]. These studies indicate that poorer mechanical properties are obtained if carbide networks are present along the prior particle boundaries (PPBs). A two-step HIP procedure resulted in a fine grained, PPB-decoration-free microstructure and improved mechanical properties[32].

The PPB precipitation in superalloys made by the powder route can also be minimized by the optimization of composition and heat treatment schedules In this regard, work at DMRL has indicated that a high boron (0 08 wt%) containing PM superalloy has significantly lower PPB precipitate networks, and as a result exhibits a higher creep rupture life[33] (Figure 19). In a related study[29], the effect of heat treatment schedules on the mechanical properties of a PM low-cobalt nickel-base superalloy was investigated. It was observed that the heat treatment which resulted in a bimodal distribution of gamma prime and discrete carbide precipitation

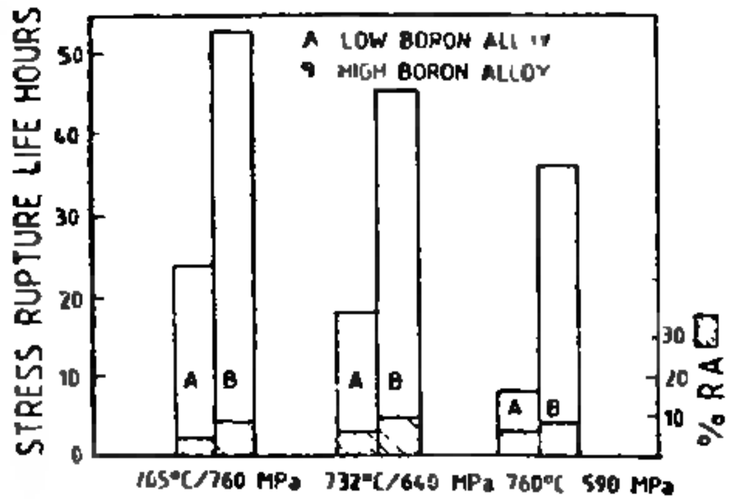

Figure 19. A comparison of stress-rupture properties of low boron (*a*), and high boron (*b*) nickel-base superalloy

at grain boundaries offered a superior combination of tensile and stress rupture properties[29].

Finite element analysis of pressure sintering of porous aggregates has been carried out at DMRL to simulate the HIP process. Using such an analysis[34] it has been possible to evaluate the local stresses, strain rates and densification rates as a function of location as well as time. A typical result from the FEM analysis indicating the sequence of pore closure and deformation pattern in a porous component undergoing isostatic pressing is illustrated in Figure 20. It has been observed that the local densification rates depend on the initial pore size, pore distribution in its neighbourhood, extent of boundary wall friction and finally on the mode of pressing (uniaxial or isostatic)[34]. This analysis in conjunction with the simple probability considerations of forces on a porous aggregate undergoing pressure sintering has also led to the concept of effective pressure[34,35].

Mechanical alloying

Mechanical alloying is a process initially developed for producing dispersion-strengthened alloys from powder blends. The process employs repeated welding, fracturing and rewelding of powder particles in a dry, high energy ball charge, to achieve an extremely deformed metastable structure which can contain dispersoids uniformly dispersed in the matrix. During mechanical alloying (MA), the welding, rewelding and homogeneous blending of the powder components take place by impact on the surface of the grinding media. Large quantity of heat is generated during the process which can enhance diffusion among the components, and can also promote

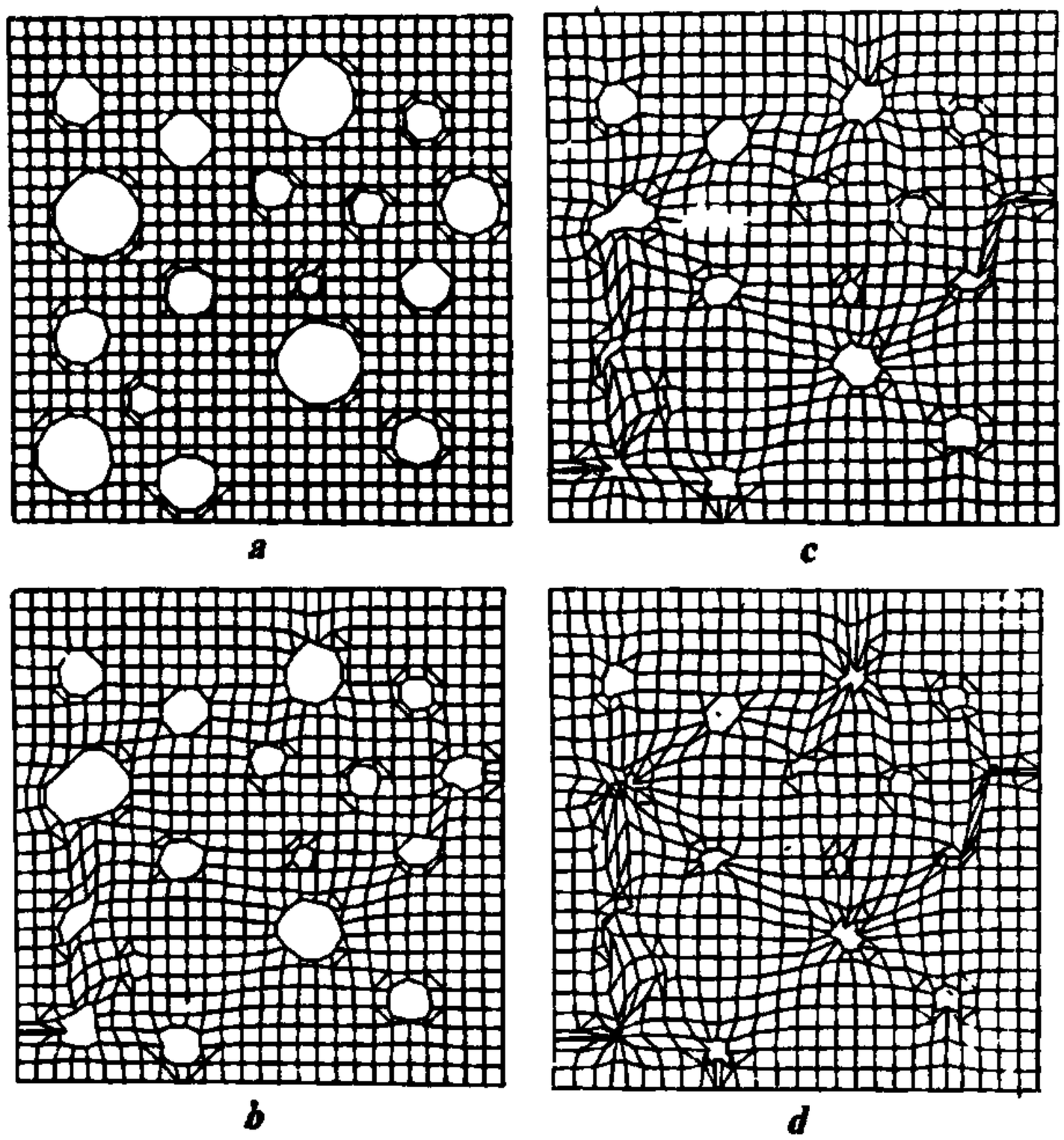

Figure 20. Sequence of pore closure and deformation pattern in a porous component, with initially rounded pores, (*a*), isostatic pressing, (*b*), uniaxial pressing, (*c*), uniaxial pressing without boundary wall friction, (*d*) with boundary wall friction.

recrystallization in the heavily cold worked powder. Thus the process offers many controls to achieve an engineered microstructure. In the one extreme, cycles of cold work and recrystallization during the process enhances diffusion and leads to alloying of the component elements[36] and is used to advantage in developing ODS nickel-base alloys with elongated grain structure. At the other extreme, with the suppression of recrystallization and the development of saturation level dislocations, an amorphous structure can result[37]. There is an almost unlimited range of microstructures between the two extremes that can be achieved in MA systems. Current research at DMRL on the system Al–Ti with carbide/oxide dispersions indicate the possibility of using the extended ductility at relatively high strain rates[38]. Other developments under investigation include high-strength composite structures.

Special test techniques

Interfacial segregation in engineering alloys using Auger electron spectroscopy

In the past Auger electron spectroscopy (AES) had been applied with much success in explaining through grain boundary chemical analysis some of the well-known embrittling phenomena, notably temper embrittlement, creep cavitation and intergranular stress corrosion cracking. More recently, the focus at DMRL has been on a relatively new theme that aims to link particular grain boundary features analysed by AES, the bulk chemical composition, the way the material has been treated and the final product properties. The emphasis is to maximize fracture resistance in terms of toughness at specified levels of strength in special engineering steels through suitable modification of grain boundary chemistry with the help of appropriate measures during the processing of the steels. An important instance in this regard is that of 17Cr–4Ni precipitation hardened stainless steel wherein the variation in impact toughness was explained in terms of grain boundary segregation of phosphorus and carbon[39,40] (Figure 21). Underlying the evolution of grain boundary chemistry are the interaction processes among trace and alloying elements (Figure 21). The ready applicability of AES to the documentation of interaction processes through measurement of grain boundary segregation isotherms (Figure 22,*a*) and determination of interaction maps (Figure 22,*b*) has been demonstrated[41–43]. The interaction processes (V-P) and (V-N) documented in Figure 21 seem to have a bearing on the uncommon beneficial effect of 'upper bainite' on toughness in upper bainite–martensite mixed microstructure[44] in a low alloy high-strength steel. It is essential to view interaction maps in association with interaction severity (index of the magnitude of interaction process)–temperature plots (Figure 23), if the effect of microstructure on grain boundary interaction processes is to be examined[45]. Another important application area where grain boundary isotherms can be employed is in eluci-

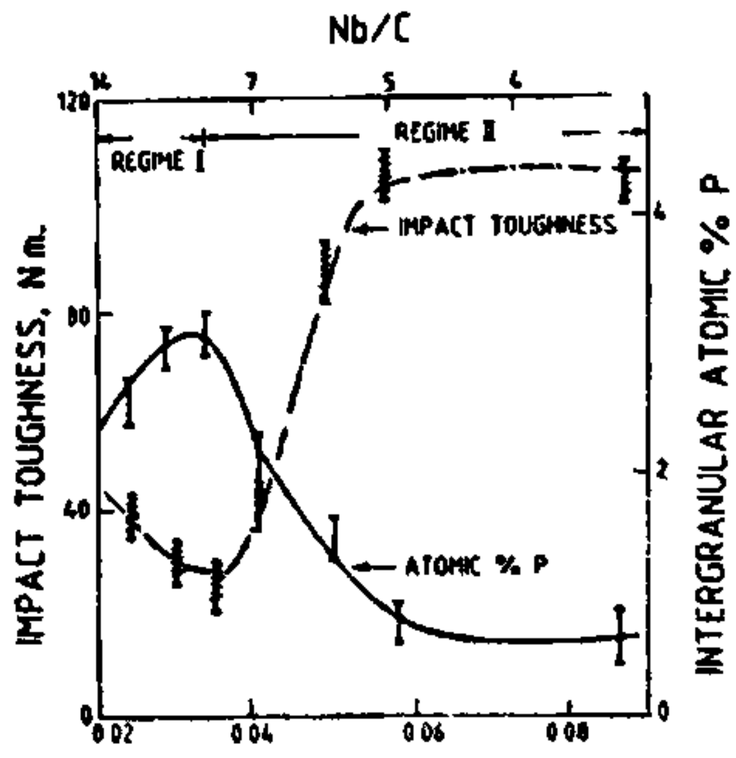

Figure 21. Impact toughness and intergranular atomic per cent phosphorus with bulk per cent carbon (also Nb/C ratio) in 17Cr 4Ni precipitation-hardened stainless steel

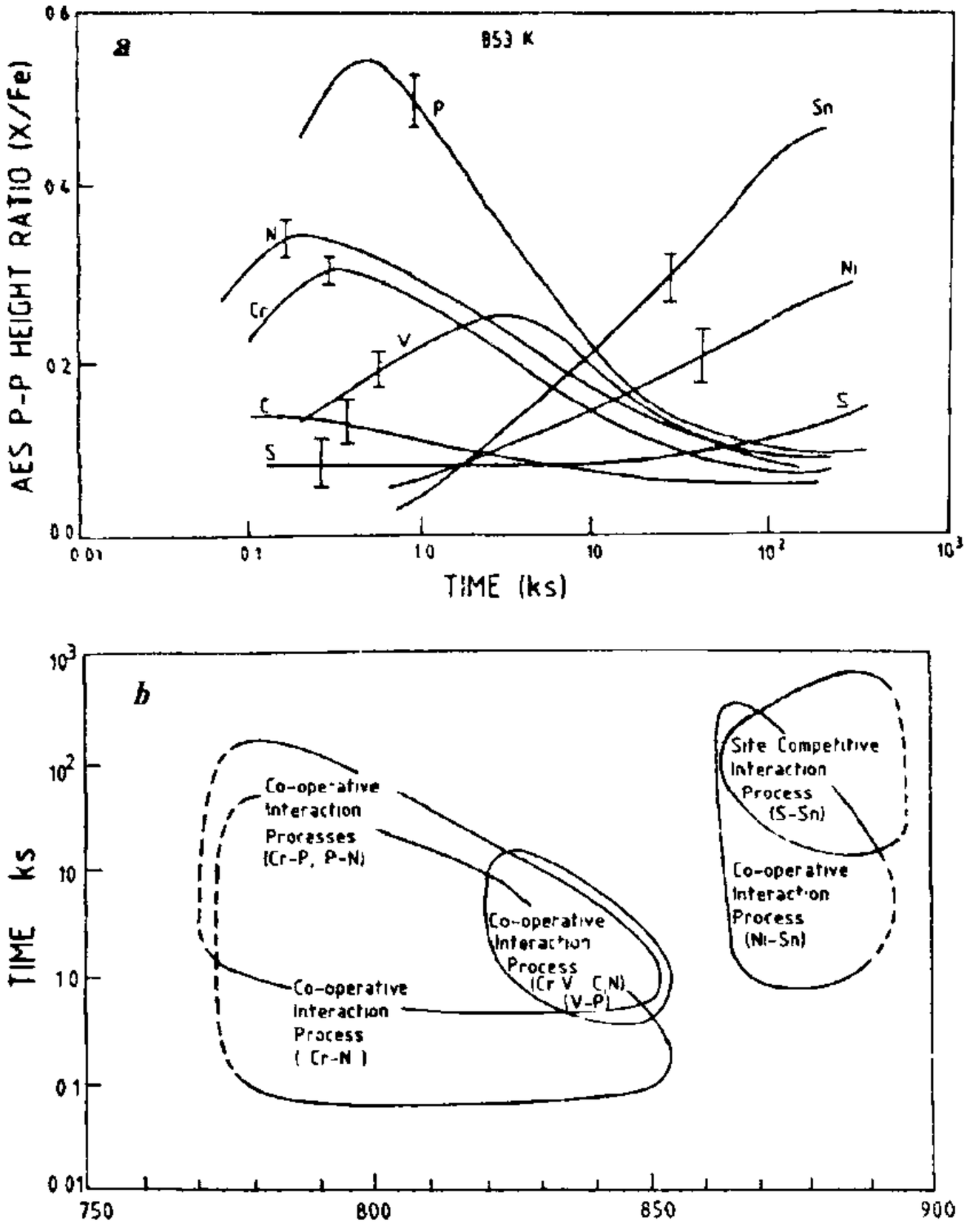

Figures 22 ***a***, Grain boundary segregation isotherms recorded at 853 K for 2 6Ni 0 4Cr - 0 28Mo–0 1 V low-alloy steel Bars indicate the range over which the values were measured. ***b***, Grain boundary interactions (interaction maps) occurring amongst trace and alloying elements in 2 6Ni–0 4Cr–0.28Mo–0 1 V low-alloy steel

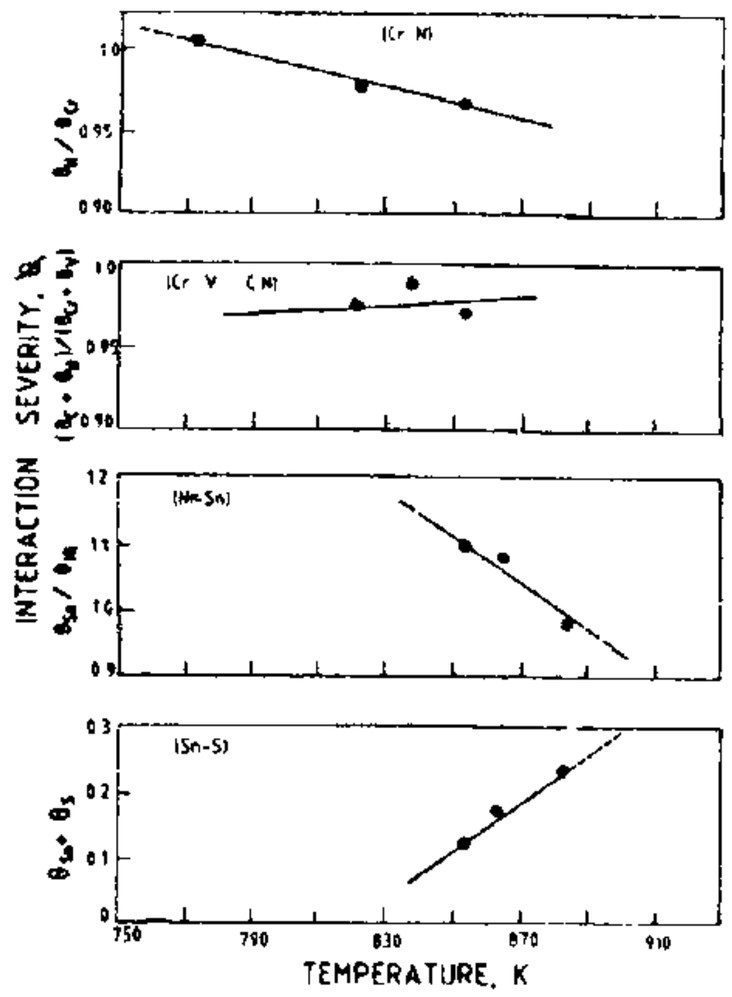

Figure 23. Interaction severity vs temperature plots for martensitic 2 6Ni 0 4Cr–0 28Mo–0 1 V low-alloy steel

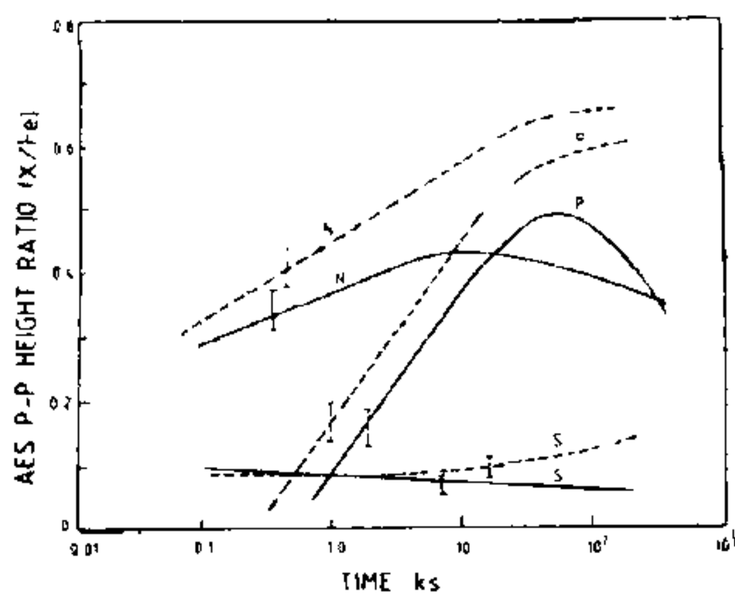

Figure 24. Segregation isotherms for P, N and S recorded at 773 K on unstressed (solid lines) and stressed (broken lines) 2.6Ni–0.4Cr–0.28Mo–0.1 V steel. Bars indicate the range over which the values were measured.

dating the role of applied stress on grain boundary chemistry[45,46] (Figure 24).

Analysis of trace elements in OFHC copper

A process for the manufacture of oxygen-free high-conductivity copper has been developed at DMRL. This has necessitated the standardization of the procedures for the analysis of a number of trace elements present in this material as a quality assurance requirement. Though direct flame/furnace atomic absorption (AAS) and the inductively coupled plasma (ICP) technique are generally used for analysing most of the elements in copper, analysis of phosphorous at three ppm level and below, and zinc and mercury at one ppm level poses special problems. Analysis of phosphorus at this level is not possible by AAS and analysis by ICP emission is severely hindered by spectral interferences[47].

To overcome these interferences a method of separation of copper and other trace constituents from phosphorus based on electrolysis and ion-exchange chromatography has been developed. Electrolysis was resorted to separate 99.9% copper by following the ASTM standard method (E–53/82) To confirm that phosphorus was not co-deposited with copper, a phosphorus-certified copper standard was also electrolysed. The electrolytes were washed and the spent solutions reduced to a volume of 5 ml by evaporation over a hot plate. The final solution in 10 m HCl was passed through ion-exchange resin column (Dowex 1–X8 200 mesh) to separate iron, residual copper and other metallic impurities, which would otherwise interfere in the phosphorus analysis. Phosphorus is absorbed on the resin and is then eluted with 10 m HCl, and phosphorus content is determined using 213.618 nm line by plasma emission spectrometric method. Phosphorus to less than 1 ppm level could be determined by this method[47].

Analysis of grain orientation in gas turbine blades

DMRL, over the last decade, has acquired considerable expertise in the manufacture of cast gas turbine blades for aircraft engine applications. In particular, DMRL has been able to produce in-house single crystal, directionally solidified (DS) and investment cast gas turbine blades of complicated, three-dimensional profiles from nickel-base superalloys. In both DS and single crystal blades, the orientation of the grain or grains has a strong influence on their mechanical behaviour, especially the creep life. This is illustrated in Table 1 for a DS, IN-100 alloy. Even a small deviation (−1 degree) of the ⟨001⟩ orientation of the grain from the stress axis causes a dramatic reduction in creep life.

The above discussion indicates the importance of the measurement of grain orientation with reference to the major stress axis in the case of DS and single crystal turbine blades on a routine basis. At DMRL, test methods based on X-ray technique have been used for this specific purpose. The results presented in Table 1 have been obtained using such an X-ray technique.

J_{IC} single-specimen technique

The *J*-integral is increasingly used as a fracture criterion for characterization of low-strength structural materials. The multiple-specimen technique for the determination of J_{IC}, the critical value of *J* near the onset of crack propagation, requires at least five specimens. It is time-consuming, expensive in terms of material requirement and testing resources. Single-specimen technique overcomes these difficulties. An application software based on partial unloading compliance has been developed at DMRL to evaluate J_{IC} using a single specimen[48] (Figure 25,*a* and *b*). Typical data obtained on mild steel are shown in Figure 25,*c*. J_{IC} value derived through the single specimen technique (227 kJ m^{-2}) matches well with that derived from the multiple specimen test data (233 kJ m^{-2}).

Table 1. Dependence of creep rupture life on grain orientation in 100 alloy at 870°C.

	Deviation of [001] from stress axis	Rupture life (h)
One grain	0 5	637
Two grains	2 & 7	270
One grain	31	136
One grain	41	139

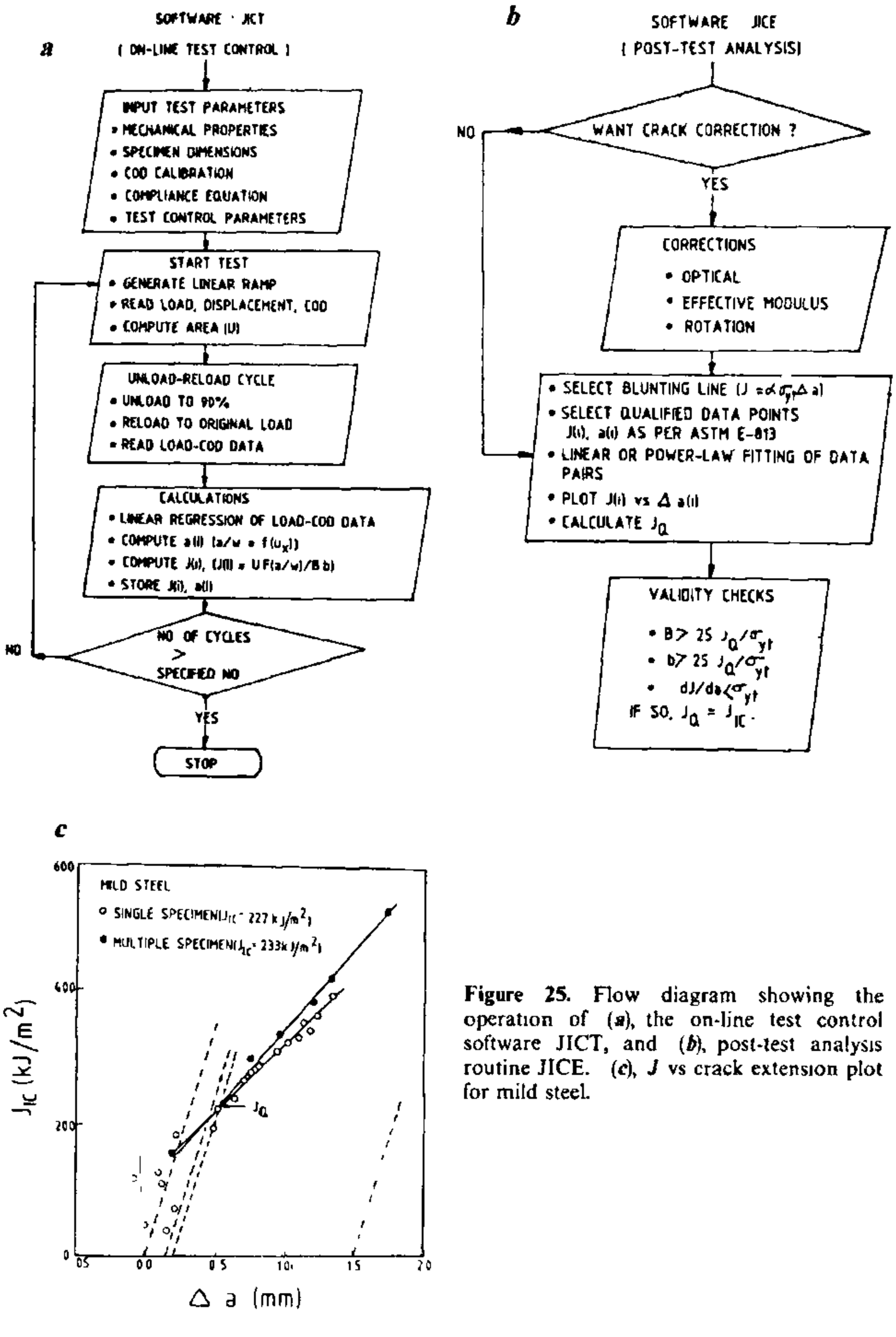

Figure 25. Flow diagram showing the operation of (*a*), the on-line test control software JICT, and (*b*), post-test analysis routine JICE. (*c*), *J* vs crack extension plot for mild steel.

Detailed research on fracture toughness of particle-free single phase materials has been undertaken at DMRL. Experimental results pertaining to the effect of grain size, test temperature and solute additions on the ductile fracture toughness J_{IC} of Armco iron are presented in Figure 26. J_{IC} increases with decreasing grain size and follows a parabolic relation with $d^{-1/2}$ while K_{IC} (K_{IC} derived from J_{IC}) varies linearly with $d^{-1/2}$ (Figure 26,*a*)[49]. The fracture toughness of bcc Armco iron is strongly dependent on test temperature[50], as illustrated in Figure 26,*b*. At lower temperatures the fracture mode changes from ductile to cleavage and is accompanied by a drastic reduction in toughness. A significant increase in fracture toughness is seen in the temperature range 383 to 573 K as a result of dynamic strain ageing (Figure 26). A further increase in temperature decreases J_{IC} and nearly attains the room temperature value at 773 K. On the other hand, the fracture toughness of fcc

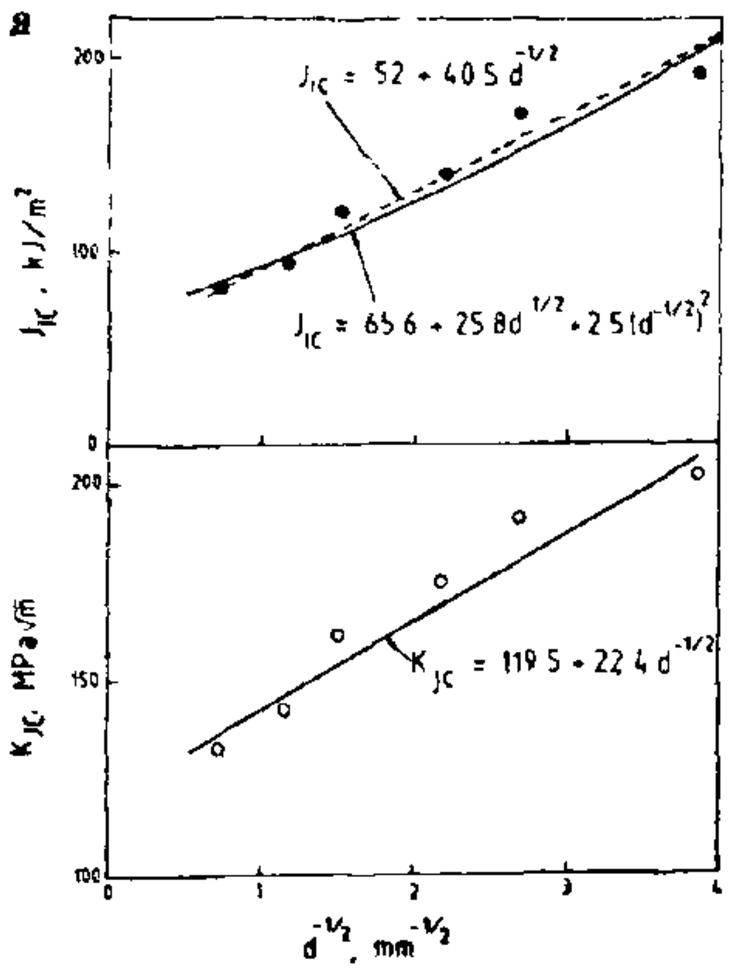

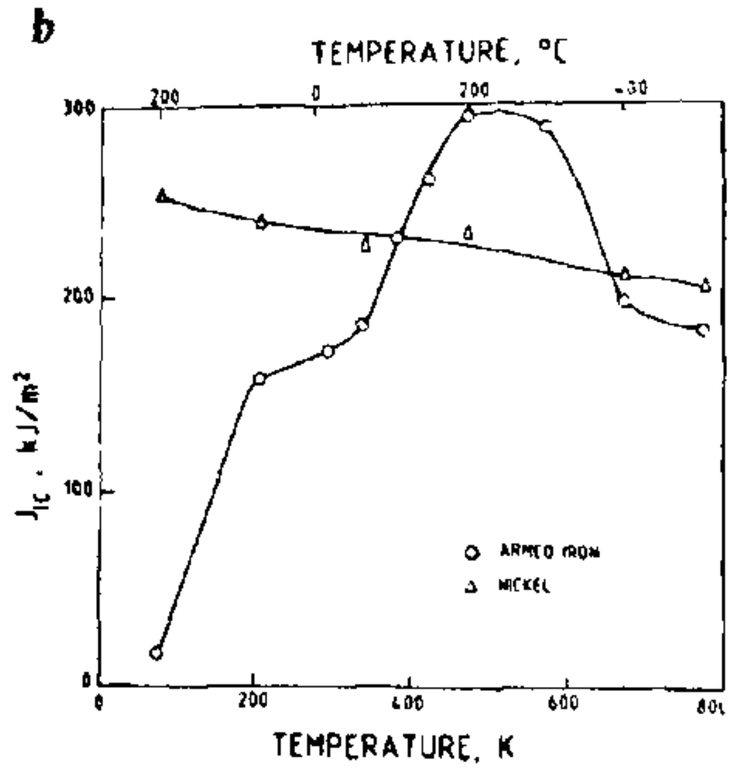

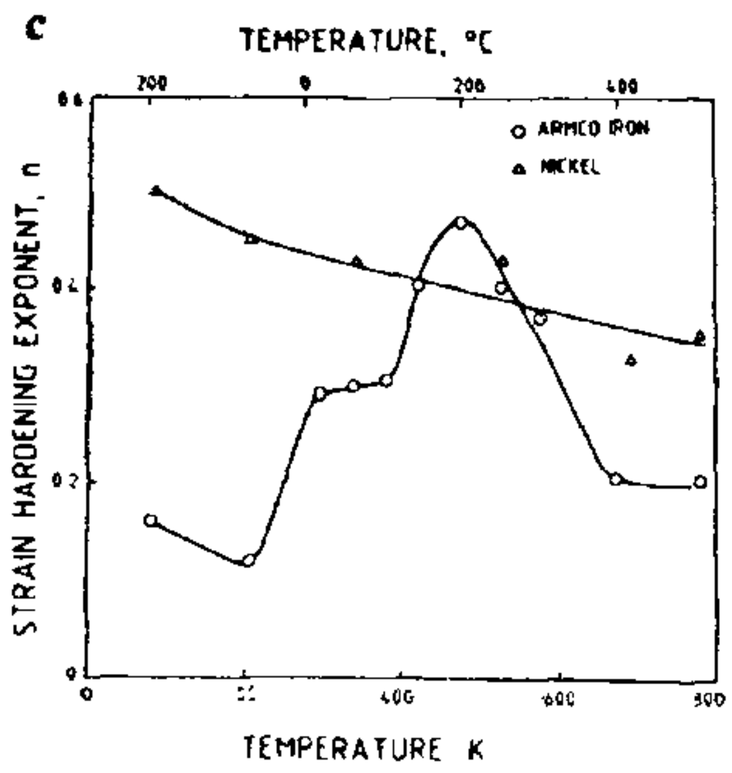

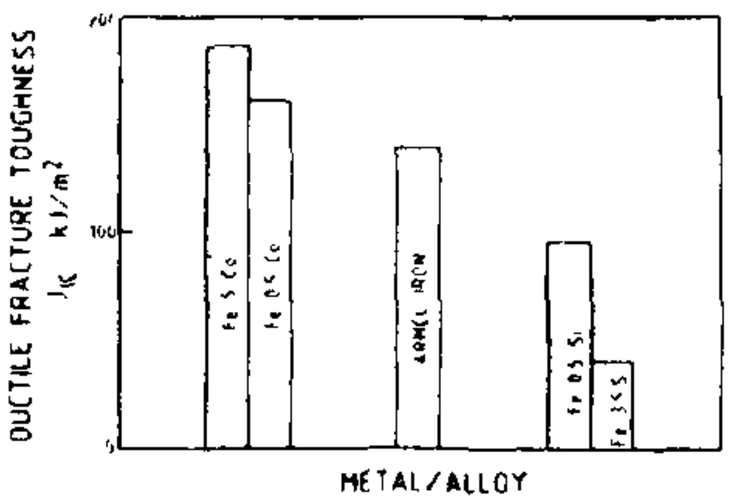

Figure 26. *a*, Variation of fracture toughness with grain size for Armco iron. *b*, Variation of fracture toughness with temperature for nickel and Armco iron. *c*, Variation of strain hardening exponent with temperature for nickel and Armco iron. *d*, Effect of solute additions on ductile fracture toughness of Armco iron

nickel is less sensitive to temperature variation and decreases gradually with the increasing temperature (Figure 26, *b*). It is interesting to note that in either case a close analogy is seen between the variation of strain hardening exponent n and the fracture toughness with temperature (Figure 26, *c*). Increase in n leads to a larger plastic zone ahead of the crack tip, which renders the crack initiation process that much more difficult leading to higher J_{IC}. Detailed investigations on the effect of solute additions on the fracture toughness of bcc iron have established that cobalt addition significantly improves toughness while silicon addition drastically decreases the same[51] (Figure 26, *d*).

Mixed-mode fracture

Most work in fracture mechanics so far has been devoted to mode I fracture. However, in most practical situations structures are subjected to complex loading and can have cracks oriented in any direction with respect to the loading axis. Also in some cases initially mode I cracks can reorient and grow under mixed-mode loading conditions. Hence, it is essential to study crack initiation and propagation under mixed-mode conditions. In recent years, experimental and theoretical studies on mixed-mode fracture are gaining momentum. Although standard test procedures are yet to emerge, in principle, one can follow procedures similar to those for mode I fracture with slight modifications in specimen design, loading fixtures and data analysis.

Currently, mixed-mode fracture behaviour of aluminium–lithium alloys is being investigated at DMRL. This has been fuelled by experimental observations of initial mode I cracks deflecting and growing under mixed-mode (mode I-mode II) conditions in the case of Alcan 8090 aluminium–lithium alloy sheets. Macroscopic crack deflections have been observed in *R*-curve sheet specimens tested in L–T orientation but not in T–L orientation. This is illustrated in Figure 27. A simple theoretical mixed-mode analysis was done to predict the increase in slow stable crack growth resistance (K_R) in L–T orientation compared to T–L orientation. It predicts[52],

$$[K_R]_{L-T} = [K_R]_{T-L} \sec \theta^{\pm},$$

where θ is the crack deflection angle. The agreement between the experimentally observed and theoretically predicted *R*-curves in L–T orientations is good. This is also illustrated in Figure 27. The implications of this analysis for Al–Li alloys are that the resistance to slow stable crack growth can be increased by controlling the microstructural features which promote large crack deflections.

High-strain rate plastic flow behaviour

A novel test technique, called the dynamic indentation (DI) technique, has been developed at DMRL to characterize the high-strain rate plastic flow behaviour of metallic materials. This technique involves impacting the test material with very hard tungsten carbide balls over a range of velocities using a single-stage gas gun as illustrated in Figure 28. The size and profile of the craters formed on a test material, as a result of the impact of the ball, are then measured. These data along with the impact velocity are then utilized to generate the flow stress-strain curve of the test material as shown elsewhere[53]. The flow stress-strain curves obtained using the DI technique actually correspond to high-strain rate, adiabatic deformation conditions as opposed to the conventional low-strain rate, isothermal flow curves obtainable from tensile tests. In Figure 29, the high-strain rate stress-strain curves typical of copper and iron obtained using the DI technique are illustrated. The static stress-strain curves are also indicated in the same figure for comparison. In the case of copper, the stress-strain curves

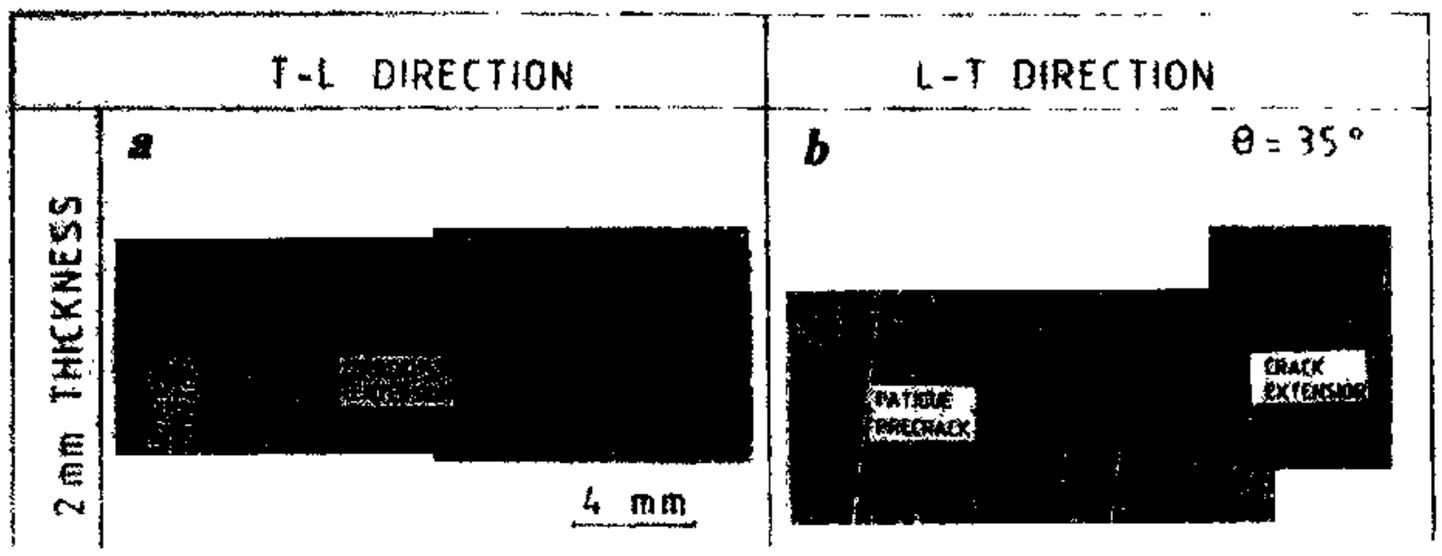

Figure 27. *a*, Crack path morphology for T–L orientation in 2 mm thick sheet. *b*, Crack path morphology for L–T orientation in 2-mm-thick sheet, *c*, Experimentally obtained *R*-curves in T–L and L–T orientations along with the theoretically predicted *R*-curve in L–T orientation in 2-mm-thick sheet (material ALCAN 8090 Al–Li alloy).

are similar at low- and high-strain rates except for the fact that it is uniformly stronger at higher strain rates. In contrast, in the case of iron, the high-strain rate flow stress increases with increasing strain, attains a peak value at a critical strain and then starts decreasing with further increase in strain. The above decrease in flow stress beyond a critical strain is due to the localization of plastic deformation as demonstrated elsewhere[53].

Solid particle erosion

Many of the components of the thermal power plants, aeroengines and pipeline-transporting slurries undergo significant erosion during service. At DMRL, two erosion test facilities, one for room temperature erosion tests and the other for tests at elevated temperatures, have been set up. A schematic view of the erosion rig is shown in Figure 30. Using this rig, erosion resistance of a variety of test materials eroded with a variety of erodent particles and at various impact angles, velocities and test temperatures have been characterized[54–57]. Figure 31, wherein the variation of the erosion rate of 304, 316 and 410 stainless steels with test temperature is illustrated[56,57], represents the typical erosion data that can be obtained.

High-speed sliding wear

Wear resistance of materials at high-sliding velocities is relevant to the development of aircraft brake pads and wear-resistant gun barrel materials or coatings. At DMRL, a friction dynamometer which can be utilized to carry out high-speed wear tests in various test configurations has been recently set up. A schematic view of the dynamometer is given in Figure 32,*a*. The main components of the dynamometer are the drive system, the hydraulic loading system and the monitoring system. To conduct the test using the dynamometer, test samples are screwed onto the stationary disc and slid against the bottom, rotating disc and the load is applied simultaneously. The load can be varied in the range 50 to 10,000 kg and can be applied either monotonically or in a cyclic fashion. In the latter case, the cycle time can be controlled in the range 10 to 1000 sec. The sliding speeds can be varied in the range 1 to 10 m sec^{-1}. During the test, the wear rate, the friction coefficient and the interface temperature are monitored continuously. The tribological behaviour of the carbon–carbon composites (self-mating) has been evaluated recently using the dynamometer. Typical friction data obtained as a part of that study are illustrated in Figure 32,*b*.

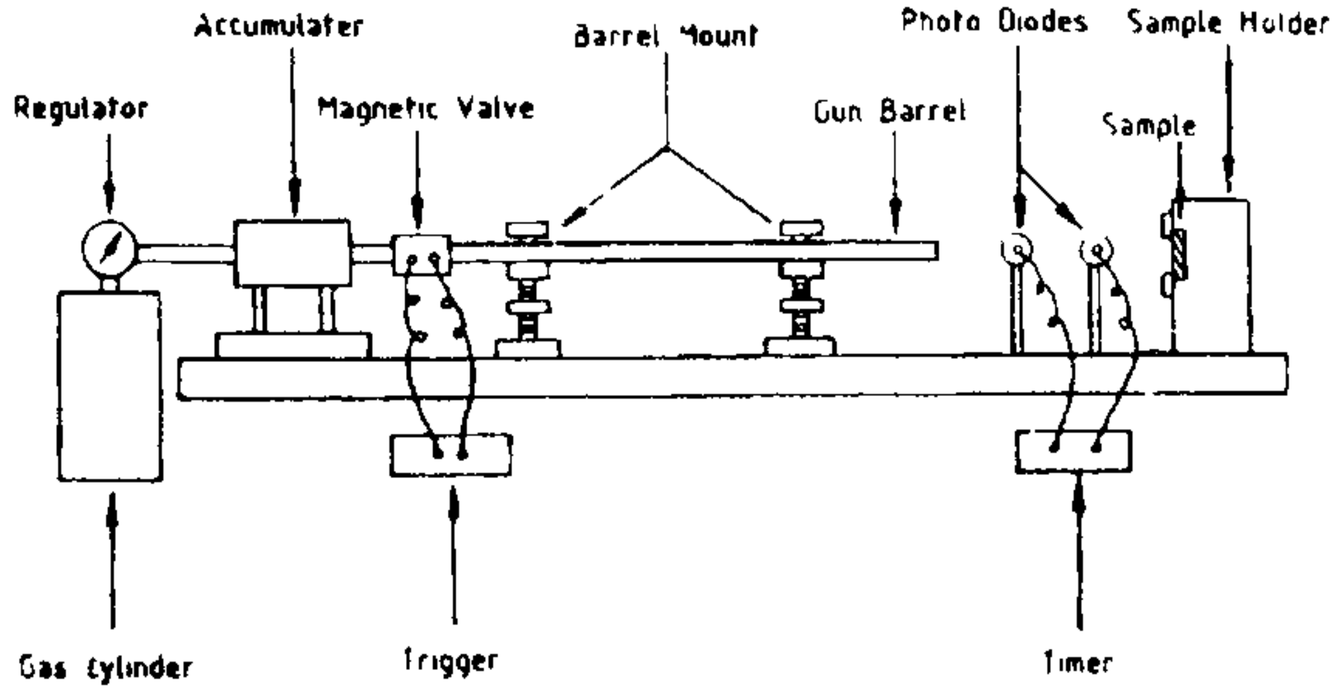

Figure 28. A schematic view of the gas gun facility utilized for carrying out dynamic indentation test.

X-ray and quantitative image processing using scanning electron microscope (SEM)

Image processing of any X-ray analog or sequential signal produced by the electron column can be carried out by Kevex advanced imaging system positioned at DMRL. Quantitative image analysis can be carried out for counting the number of particles, area perimeter, etc. The following example illustrates the use of quantitative image analysis. The W-Ni Fe liquid phase sintered alloy samples which exhibited a wide

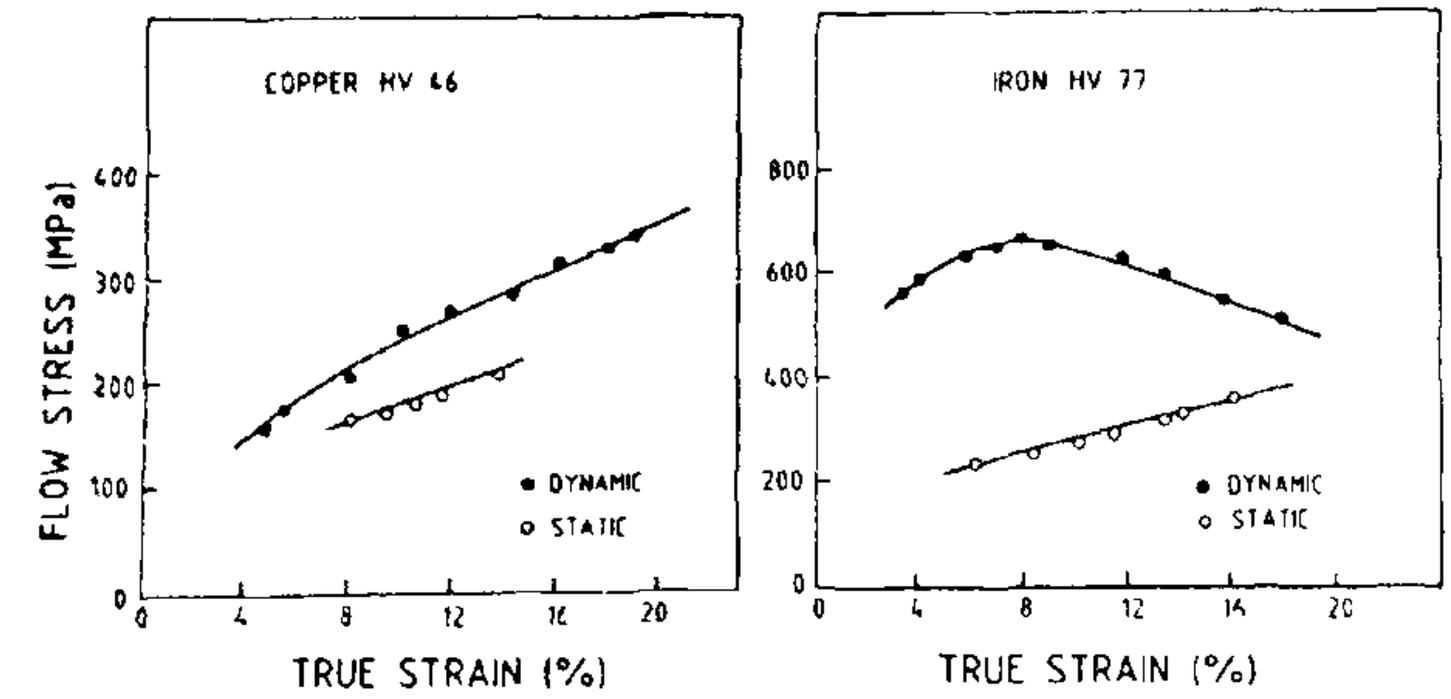

Figure 29. The dynamic flow stress-strain behaviour (filled circles) of copper and iron obtained using the DI technique compared with the static flow behaviour (unfilled circles).

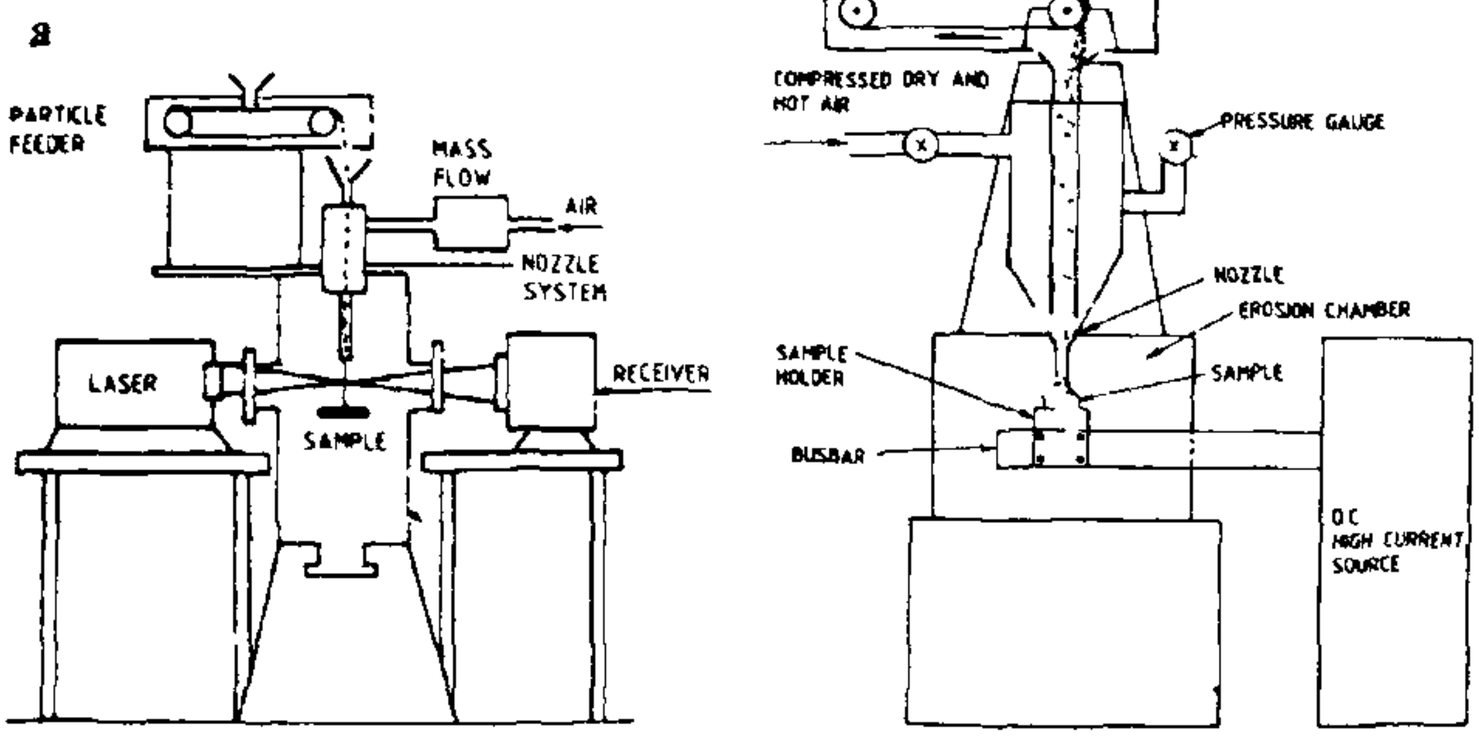

Figure 30. Schematic views of the room temperature (*a*), and high temperature (*b*) solid particle erosion test facilities.

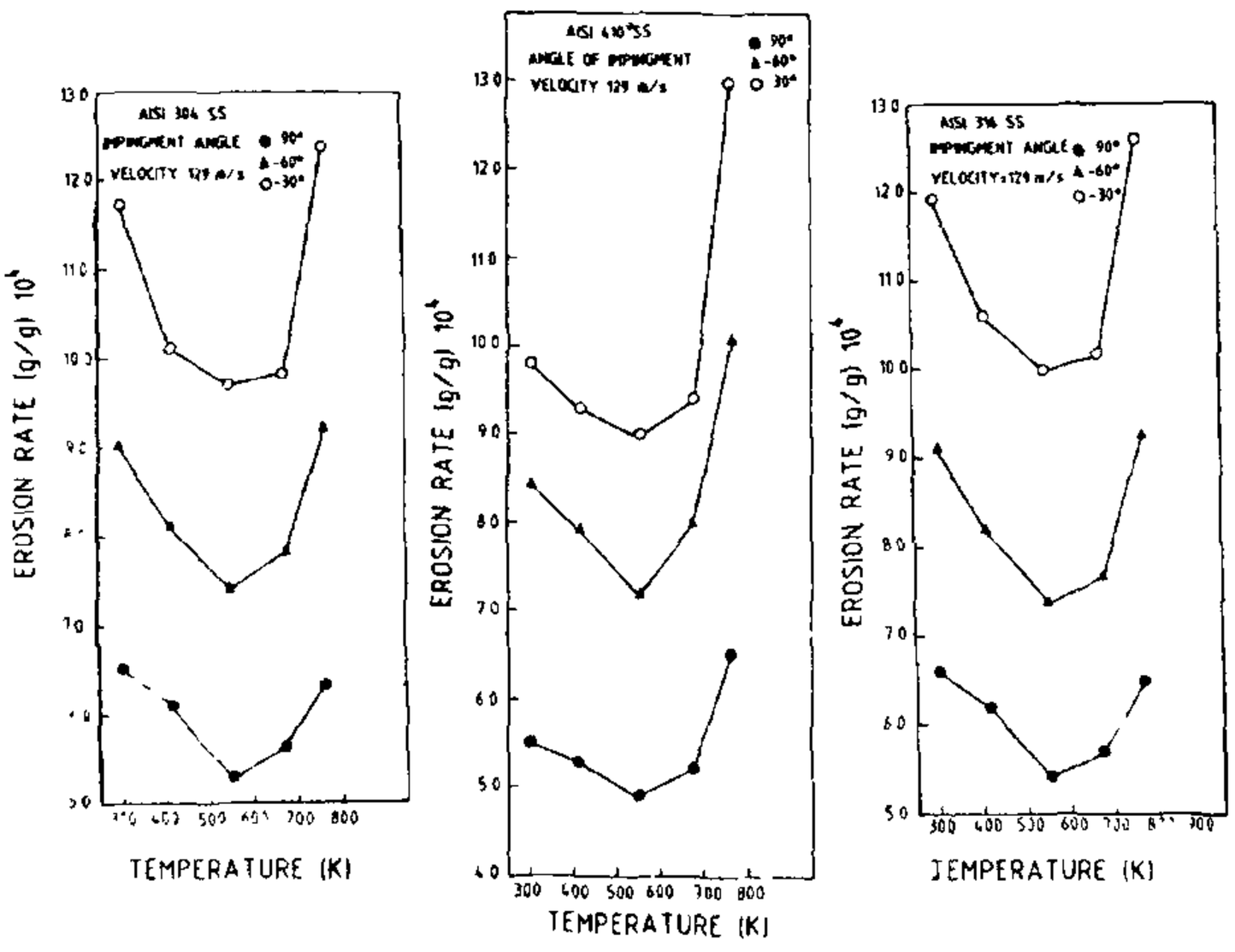

Figure 31. The effect of test temperature on the solid particle erosion behaviour of 304, 410 and 316 stainless steels (impact velocity 129 m sec^{-1}; SiC erodent)

range with respect to tensile ductility were examined to estimate the size of the W particle and volume fraction of the matrix phase using the image analysis system of the Jeol SEM. Images were acquired in the Kevex using advanced imaging techniques, and quantitative feature analysis was carried out The above image and feature analysis indicated a correlation between the tungsten particle size and tensile elongation as illustrated in Figure 33.

Convergent beam electron diffraction and channelling-enhanced micro analysis using the transmission electron microscope

The convergent beam electron diffraction (CBED) technique use a converging beam of electrons focused on to the specimen in a transmission electron microscope (TEM). This technique helps in determining the crystal symmetry and space group by observing the symmetries exhibited by the diffracting crystal in high-symmetry zone axes. Since Friedel's law breaks down for electron diffraction, this technique is also suited for determining the lack of centre of inversion. At DMRL, using CBED, an orthorhombic phase has been identified in the Ti–Al–Nb system as indicated earlier in the section on intermetallics. More recently, it has been shown[58] that a hydrogen-induced phase transformation can convert the α_2 phase to an orthorhombic phase. However, in this transformed phase, there is no definite Nb-sublattice as indicated by the [001] CBED pattern in Figure 34.

Channelling-enhanced microanalysis is ideally suited for the determination of site occupation of a specific species in a known superstructure. At DMRL, using the above technique, the site occupation for a number of elements has been determined in two-ordered intermetallics, namely $Ti_3Al(DO_{19})$ and Ti_2AlNb (B2)[6]. In this technique, the crystal is oriented in a 2-beam condition and energy dispersive spectroscopy (EDS) peaks are compared for various deviation parameters (*s*). The ratio of intensities obtained for at least two *s* values and also in the non-channelling condition can then be used to determine the specific site occupation. Some results obtained in the above manner are given in Table 2.

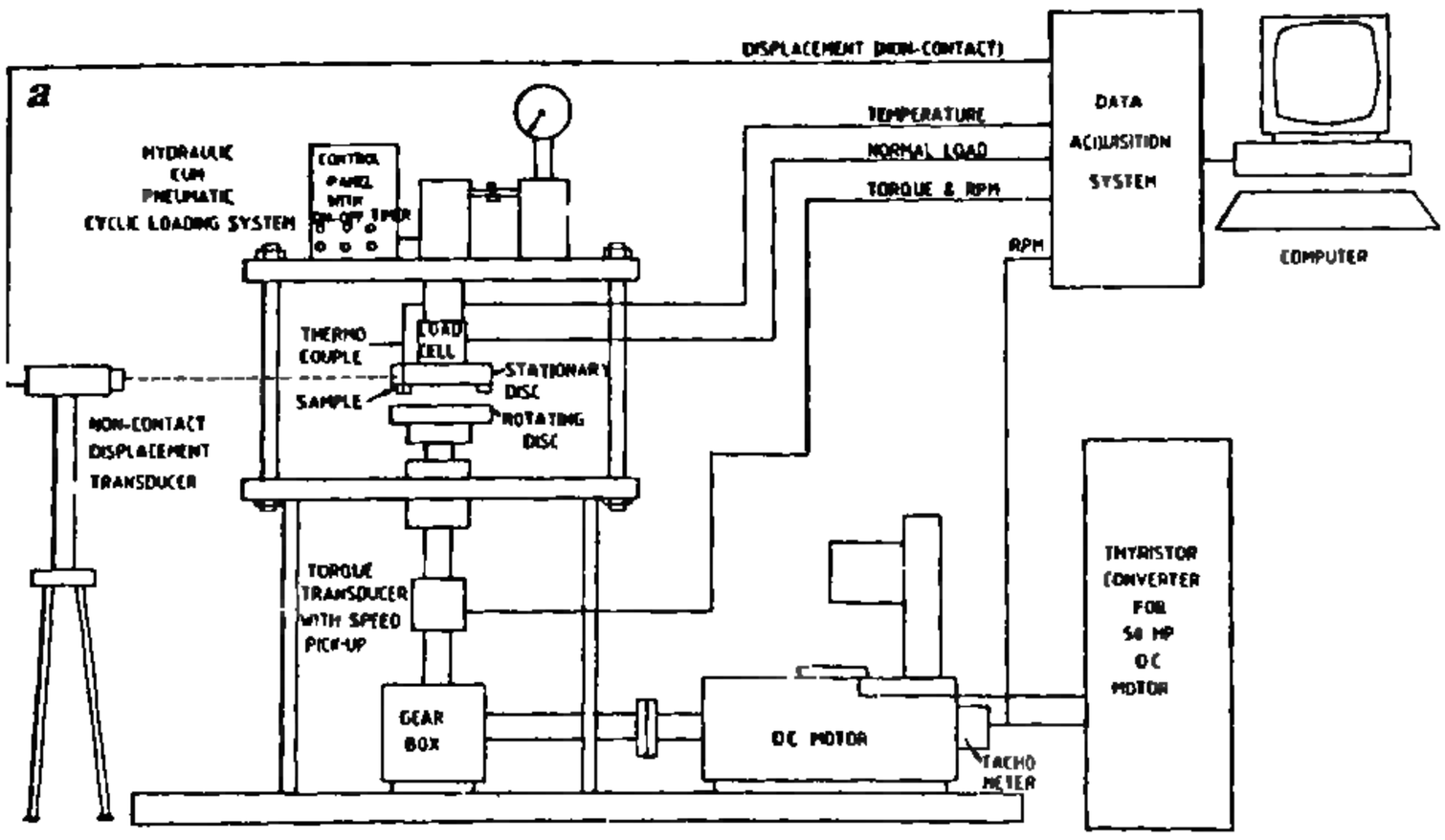

Figure 32. ***a,*** A schematic view of the friction dynamometer capable of characterizing the tribological behaviour at high sliding speeds. ***b,*** Typical friction data obtained for carbon–carbon composites (self-mating).

Other research activities

In addition to the research work discussed in the last three sections, considerable work has been carried out in a number of related and complementary areas. In the area of new materials, extensive work on the solidification behaviour, structure and mechanical properties of quasicrystals[59–62], thermal, mechanical and electrochemical behaviour of metallic glasses[63–72], structure–mechanical property correlations in newer steels[39,44,95] and the toughening mechanisms in alumina–silicon carbide ceramic matrix composites[73] has been performed. DMRL has developed considerable expertise in the area of superplastic forming of titanium aluminides[74] and titanium alloys[75,76]. Surface modification of titanium alloys through the use of laser[77] and explosive compacting of high expansion alloys[78] typify the novel areas of materials processing wherein work is in progress.

Another area where considerable work has been done pertains to the analytical and numerical modelling of a variety of processes and phenomena. Examples of such work during the last three years, include the modelling of high-temperature creep deformation[79], intergranular creep fracture[80–82], the dynamics of high velocity impacts[83–85], erosive and abrasive wear[86–88] and rapid solidification[89,90]. The participation of DMRL in the 'ASM–NBS phase diagram' programme and the evaluation of 90 binary phase diagrams of the tungsten system[91–94] as a part of this programme deserve mention.

Approach to future R&D

In conclusion it is gratifying to state that over the years DMRL has made tangible progress in technology in terms of product and process development on the one hand, and on the other in regard to basic research supported by modern test techniques. The work of DMRL in both these spheres has by and large found acceptance. We have referred to, in the above report, the products and processes developed by DMRL that have actually gone into service not only in defence but also in civilian sectors. Similarly, DMRL research has been published in refereed and reputed journals. These two activities, namely technology for product/process development and original re-

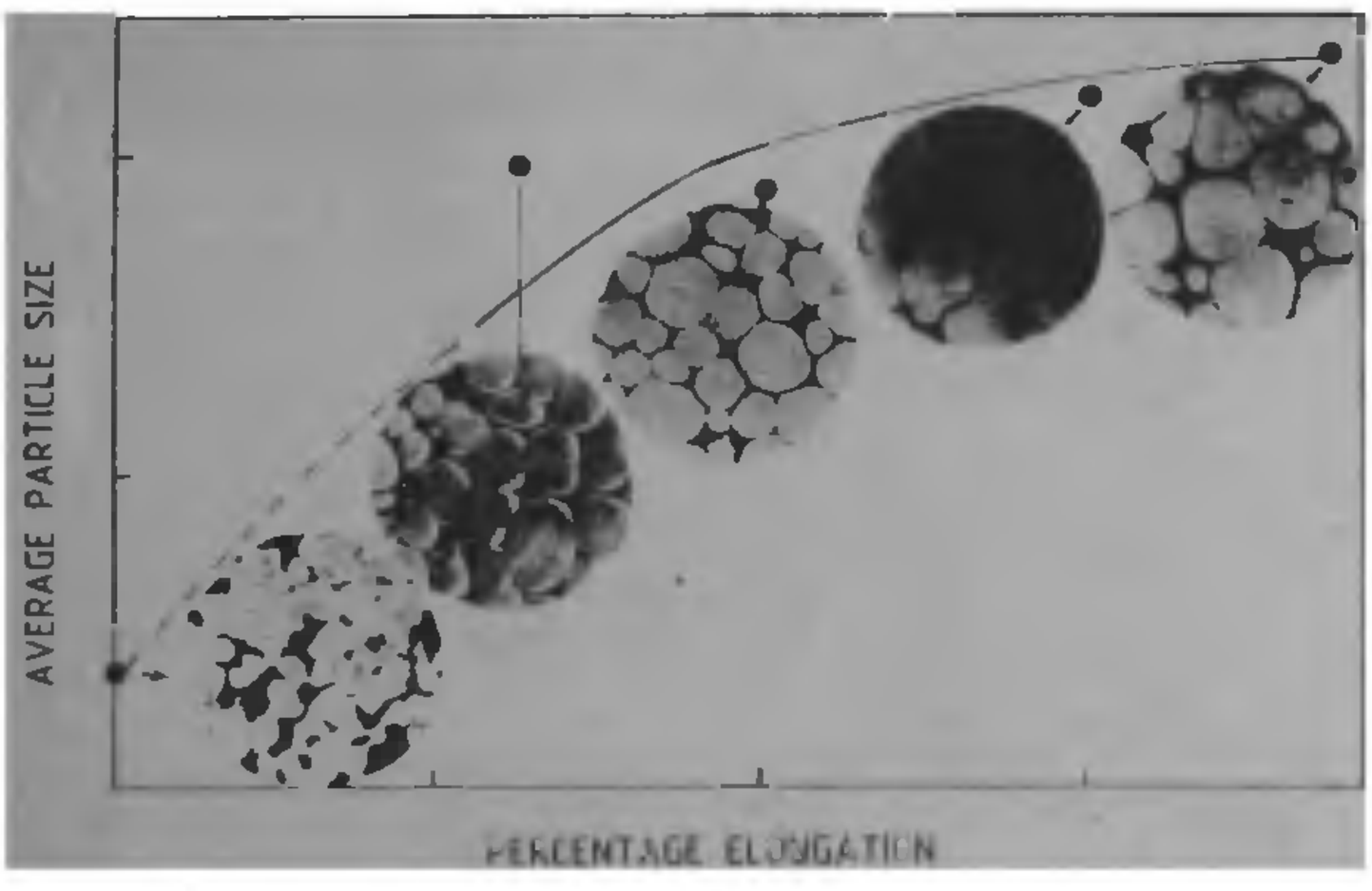

Figure 33. Correlation of tungsten particle size with per cent elongation

Table 2. Site substitution behaviour of a number of elements in the intermetallics Ti_3Al (DO_{19}) and β_0(B2)

THERMODYNAMIC MODEL + CHANNELLING-ENHANCED X-RAY MICROANALYSIS → SITE SUBSTITUTION BEHAVIOUR

Ti_3Al (DO_{19})		β_0(B2)	
Ti sites	Al sites	Ti sites	Al Nb sites
Hf	Co (?)		Mo
Zr		Zr	Co
Mo		Hf	V
Nb			

? No solubility

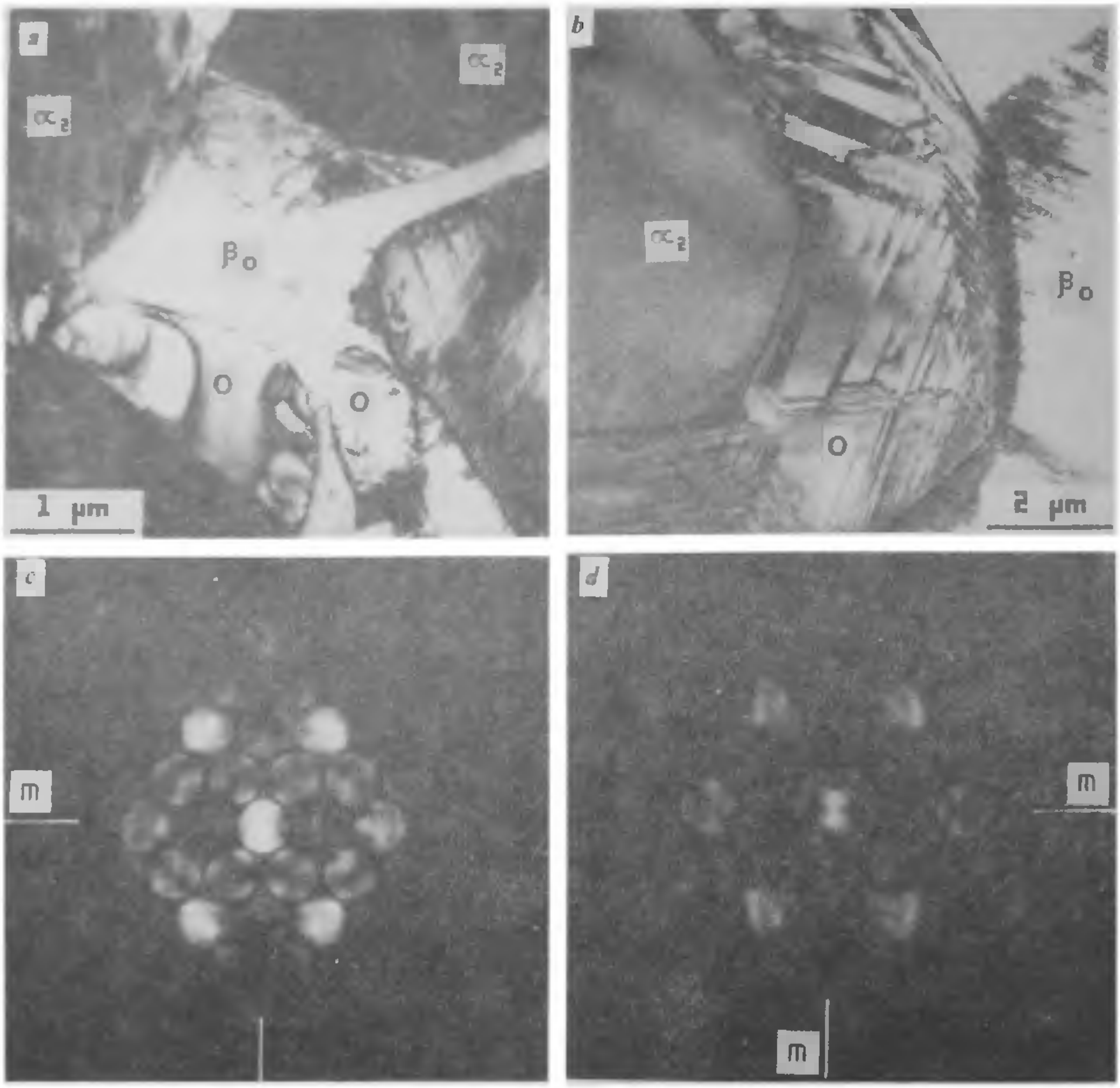

Figure 34. Orthorhombic distortions of the phase in a Ti-24 at per cent Al-15 at per cent Nb alloy Facts and artefacts. *a*, Orthorhombic phase occurring as an equilibrium phase. *b*, Arising out of hydrogen pick-up during thin foil preparation. *c*, [001] CBED from 'O' phase in *a*. Notice the non-uniform intensities spots showing definite Nb sublattice occupancy in the compound Ti_2AlNb. *d*, P[001] CBED pattern from the hydrogen-induced phase. Nb occupies the Ti sublattice in $(Ti,Nb)_3Al$ as evident from equal intensities of the spots next to the transmitted beam

search for new understanding of material behaviour, needless to say, often call for distinctly different skills Even so every endeavour has been made at DMRL to sustain a certain relationship, perhaps not in a structured form. The experience has been that often the research expertise has been tapped at the stage of the final delivery of the product process or upgradation of the same. It is also noteworthy that many of the special test techniques were developed specifically with a view to characterize the behaviour of materials under conditions that simulate the environment in actual application. However, we have been meaning to strive to bring about an altogether new form of juxtaposition of research and technology—as we realize more and more the imperative of creative research feeding into the product and process development from conceptualization to commercialization. What is needed for this is an appropriate culture that can bring about *research-driven development*. It is earnestly hoped that the current ambience and striving by DMRL staff and scientists will generate such a culture the permeating influence of which is so essential, for the

aim is to register notable firsts in materials technology in the international context.

1. Gogia, A. K., Ph.D thesis, Defence Metallurgical Research Laboratory and Banaras Hindu University, India, 1990.
2. Gogia, A. K., Banerjee, D. and Nandy, T. K., *Metall. Trans.*, 1990, **A21**, 609.
3. Banerjee, D., Gogia, A. K. and Nandy, T. K., *Metall. Trans.*, 1990, **A21**, 627.
4. Banerjee, D., Gogia, A. K., Nandy, T. K. and Joshi, V. A., *Acta Metall.*, 1988, **36**, 871.
5. Banerjee, D., Nandy, T. K. and Gogia, A. K., *Scr. Metall.*, 1987, **21**, 597.
6. Nandy, T. K., Banerjee, D. and Gogia, A. K., *Proc. 6th Int. Conf. Ti and its Alloys*, Cannes, 1988, p. 943.
7. Banerjee, D., Nandy, T. K., Gogia, A. K. and Muraleedharan, K., *Proc. 6th Int. Conf. Ti and its Alloys*, Cannes, 1988, p. 1091.
8. Nandy, T. K., unpublished research, DMRL, Hyderabad, 1990.
9. Mishra, R. S. and Banerjee, D., *Mater. Sci. Engg.*, 1990, (in press).
10. Gogia, A. K., Banerjee, D. and Nandy, T. K., unpublished research, DMRL, Hyderabad, 1989.
11. Banerjee, D. and Sundararajan, G., *Indian J. Technol.*, 1990, **28**, 259.
12. Sagar, P. K., Sundararajan, G. and Bhatia, M. L., *Scr. Metall.*, 1990, **24**, 257.
13. Pandey, M. C. and Rama Rao, P., unpublished research, DMRL, Hyderabad, 1990.
14. Pandey, M. C. and Rama Rao, P., *Scr. Metall.*, 1988, **22**, 1201.
15. Pandey, M. C. and Rama Rao, P., *Scr. Metall.*, 1989, **23**, 59.
16. Pandey, M. C., Taplin, D. M. R. and Rama Rao, P., *Mater. Sci. Engg.*, 1989, **A118**, 33.
17. Singh, R. K. and Chakravorty, C. R., *Trans. Indian Inst. Met*, 1988, **41**, 153.
18. Singh, R K. and Mishra, R. S., *Scr. Metall.*, 1990, **24**, 451.
19. Chakravorty, C. R., Vijaya Singh and Gokhale, A, *Proc 36th Annual Convention, IIF*, 1987, p. 135.
20. Gokhale, A, Vijaya Singh, Deep Kumar and Chakravorty, C. R., *Proc. Seminar on Science and Tech. of Al–Li Alloys* March 1989, p. 125.
21. Eswara Prasad, N, Malakondaiah, G. and Rama Rao, P., unpublished research, 1990.
22. Mahajan, Y. R., Satyaprasad, K. and Bhanuprasad, V. V., unpublished research, DMRL, 1990.
23. Pandey, A. B., Mishra, R. S., Mahajan, Y. R., *Scr. Metall.*, 1990, **24**, 1565.
24. Das, D. K. and Sivakumar, R., *Acta Metall. Mater. Part I*, 1990, (in press).
25. Das, D. K. and Sivakumar, R., *Acta Metall. Mater., Part II*, 1990, (in press).
26. Saha, R. L., Nandy, T. K., Misra, R. D. K. and Jacob, K. T., *Bull. Mater. Sci.*, 1989, **12**, 481.
27. Saha, R. L., Nandy, T. K., Misra, R. D. K. and Jacob, K. T., *AFS. Trans.*, 1990, (in press).
28. Saha, R. L., Nandy, T. K., Misra, R. D. K. and Jacob, K. T., *Met. Trans.*, 1990, **B21**, 559.
29. Sharma, K. K. and Tewari, S. N., *Int. J. Powder Metall.*, 1988, **24**, 13.
30. Sekhar, J. A., Mohan, M., Divakar, C. and Singh, A. K., *Scr. Metall.*, 1984, **18**, 1327.
31. Arunachalam V. S. and Sundaresan R., in *Materials Science and Technology Series* (ed. Cahn, R. W.), VCH Verlagsgellschaft, W. Germany, 1990, Vol. 15, Ch. 9.
32. Prakash, T. L., Chari, Y. N., Bhagiradha Rao, E. S. and Thamburaj, R., *Metall. Trans.*, 1983, **A14**, 733.
33. Sharma, K. K., Tewari, S. N., Birla, N. C. and Misra, R. S., *Powder Metall.*, 1988, **31**, 52.
34 Rama Krishnan, N., Balakrishna Bhat, T. and Arunachalam, V. S., *Acta. Metall.*, 1984, **32**, 357.
35. Balakrishna Bhat, T., Ramakrishnan, N. and Arunachalam, V. S., *Scr. Metall.*, 1981, **15**, 339.
36. Bhagiradha Rao, E. S., in *Powder Metallurgy—Recent Advances* (ed. Arunachalam, V. S. and Raman, O. V.), Oxford and IBH Pubshing, 1989, pp. 28–45.
37. Sundaresan, R., Jackson, A. G., Krishnamurthy, S. and Froes, F. H., *Mater. Sci. Engg*, 1988, **97**, 115.
38. Sonawane, P. W., Krishna Swamy, W., Sundaresan, R. and Birla, N. C., presented at ASM conf. on Structural Applications of Mechanical Alloying, Myrtle Beach, March, 1990.
39 Misra, R D. K., Prasad, C. Y., Balasubramanian, T. V. and Rama Rao, P., *Scr. Metall.*, 1986, **20**, 713.
40. Misra, R. D. K., Prasad, C. Y., Balasubramanian, T. V. and Rama Rao, P., *Scr. Metall.*, 1986, **20**, 1339.
41. Misra, R. D K and Rama Rao, P., *Indian J. Technol.*, (special issue) 1990, **28**, 500.
42. Misra, R. D K., Balasubramanian, T. V. and Rama Rao, P., *Acta Metall.*, 1987, **35**, 2995.
43 Misra, R. D. K. and Balasubramanian, T. V., *Acta Metall.*, 1989, **37**, 1475.
44. Narasimha Rao, T. V. L., Dikshit, S. N., Malakondaiah, G. and Rama Rao, P., *Scr. Metall.*, 1990, **24**, 1323.
45. Misra, R. D. K. and Balasubramanian, T. V., *Acta Metall. Mater.*, 1990 (in press).
46. Misra, R. D. K. and Balasubramanian, T. V., *Acta Metall. Mater.*, 1990, **38**, 1263.
47. Lalitha Kumari, V., Rukmani Desikan, N., Athavale, S. V. and Rao, T. H., *Trans. Indian Inst. Met.*, 1989, **42**, 325.
48. Srinivas, M., Malakondaiah, G. and Rama Rao, P., *Engg. Fracture Mech.*, 1987, **28**, 561.
49 Srinivas, M., Malakondaiah, G., Armstrong, R. W. and Rama Rao, P., *Acta Metall. Mater.*, 1991, (in press).
50. Srinivas, M., Malakondaiah, G. and Rama Rao, P., unpublished work DMRL, 1990.
51. Srinivas, M., Malakondaiah, G. and Rama Rao, P., *Bull. Mater. Sci.*, 1988, **11**, 329.
52. Kamat, S. V. and Eswara Prasad, N., *Scr. Metall. Mater.*, 1990, **24**, 1907.
53. Tirupataiah, Y. and Sundararajan, G., *J. Mech. Phys. Solids*, 1990, (in press).
54. Venugopal Reddy, A., Sundararajan, G., Sivakumar, R. and Rama Rao, P., *Acta Metall.*, 1984, **32**, 1305.
55. Venugopal Reddy, A. and Sundararajan, G., *Metall. Trans.*, 1987, **A18**, 35.
56. Trilok Singh and Sundararajan, G., *Met. Trans. A*, 1990, (in press).
57. Trilok Singh, Tiwari, S. N. and Sundararajan, G., *Wear*, 1990, (in press).
58. Muraleedharan, K., Nagendra Naidu, S. V. and Banerjee, D., *Scr. Metall. Mat.*, 1990, **24**, 27.
59. Gopalan, R., Akhtar, D. and Rajasekharan, T., *Z. Metallkunde*, 1990, **81**, 111.
60. Bhaduri, S. B. and Sekhar, J. A., *Nature*, 1987, **327**, 609.
61. Rajasekharan, T., Gopalan, R., Akhtar, D. and Banerjee, D., *Scr. Metal.*, 1987, **21**, 289.
62. Rao, K. N. and Sekhar, J. A., *Scr. Metal*, 1987, **21**, 905.
63. Reddy, P. V. and Akhtar, D., *J. Less Common Metals*, 1988, **138**, L5.
64. Reddy, P. V. and Akhtar, D., *Phys. Status Solidi*, 1987, **102**, K105.
65. Akhtar, D. and Misra, R. D. K., *Scr Metall.*, 1986, **20**, 627.
66. Misra, R. D K. and Akhtar, D., *Mater. Res. Bull.*, 1986, **21**, 593, 1473.
67. Misra, R D. K. and Akhtar, D., *Z. Metallkunde*, 1986, **77**, 417.
68. Akhtar, D., Misra, R. D. K. and Bhaduri, S. B., *Acta Metall.*, 1986, **34**, 1307.
69 Akhtar, D. and Mathur, R. P, *J. Mater. Sci*, 1987, **22**, 2509.
70. Akhtar, D and Mathur, R P., *Z. Metallkunde*, 1987, **78**, 738.
71. Akhtar, D. and Mathur, R. P., *J. Mater. Sci.*, 1987, **22**, 2158.
72. Misra, R. D. K. and Akhtar, D., *Mater. Sci. Engg.*, 1987, **92**, 207.
73. Chakravorty, A., Bhaduri, S. B. and Mahajan, Y. R., *Advances in Fracture Research ICF7* (eds. Salama, K., Ravichander, K., Taplin, D. M. R and Rama Rao, P.), Pergamon Press, 1989, p. 2905.
74. Dutta, A. and Banerjee, D., *Scr. Met.*

Mater., 1990, **24**, 1319
75 Dutta, A and Birla, N C., *Mater Sci Technol.*, 1988, **4**, 341
76 Dutta, A and Birla, N. C, *Scr Met.*, 1987, **21**, 1051
77 Bharti, A., Sivakumar, R. and Goel, D B. *J Laser Appl.*, 1989, **1**, 45
78 Mahendra Kumar, *Powder Met Sci. Technol.*, 1989, **1**, 12
79 Malakondaiah, G., Prasad, N., Sundararajan, G and Rama Rao, P., *Acta Metal.*, 1988, **36**, 2167
80 Venkataraman, B and Sundararajan, G., *Mater. Sci. Engg.*, 1987, **92**, 113
81 Sundararajan, G., *Mater. Sci. Engg*, 1989, **A112**, 205.
82. Venkataraman, B and Sundararajan, G., *Advances in Fracture Research ICF7* (eds Salama, K., Ravichandar, K., Taplin, D. M R. and Rama Rao, P), Pergamon Press, 1989, p 1851.
83. Sundararajan, G., *Int J. Impact Engg.*, 1990, **9**, (in press).
84 Tirupataiah, Y. and Sundararajan, G., *Int. J. Impact Engg.*, 1990, **9**, 237.
85. Tirupataiah, Y., Venkataraman, B. and Sundararajan, G., *Mater. Sci Engg.*, 1990, **A124**, 133.
86 Sundararajan, G., Manish Roy and Venkataraman, B., *Wear*, 1990, (in press).
87. Sundararajan, G., *Wear*, 1990, (in press)
88. Sundararajan, G., *Wear*, 1987, **117**, 1.
89. Reddy, G. S. and Sekhar, J. A., *Acta Metall.*, 1989, **37**, 1509.
90. Rama Rao, K. V. and Sekhar, J. A., *Acta Metall*, 1987, **35**, 81.
91. Nagender Naidu, S. V. and Rama Rao, P (eds), *Monograph on Phase Diagrams of Binary Tungsten Alloys*, under preparation.
92. Nagender Naidu, S. V., Sreeramamurthy, A. M. and Rama Rao, P, *J. Alloy Phase Diagrams*, 1986, **2**, 176.
93. Nagender Naidu, S. V., Sreeramamurthy, A. M and Rama Rao, P., *Bull. Alloy Phase Diagrams*, 1984, **5**, 289.
94. Pandian, S., Nagender Naidu, S. V. and Rama Rao, P., *J. Alloy Phase Diagrams*, 1988, **4**, 73.
95. Rama Rao, P. and Kutumba Rao, V., *Int. Mater. Rev.*, 1989, **34**, 69.